THE ASTROPHYSICAL JOURNAL, 433:533–552, 1994 October 1

SPECTRAL ENERGY DISTRIBUTIONS OF THE BRIGHTEST PALOMAR-GREEN QUASARS AT INTERMEDIATE REDSHIFTS

TODD M. TRIPP
Washburn Observatory, University of Wisconsin-Madison, 475 N. Charter Street, Madison, WI 53706-1582;
E-mail: tripp@madraf.astro.wisc.edu

JILL BECHTOLD[1]
Steward Observatory, University of Arizona, Tucson, AZ 85721;
E-mail: jbechtold@as.arizona.edu

AND

RICHARD F. GREEN[1]
National Optical Astronomy Observatories,[2] P.O. Box 26732, Tucson, AZ 85726;
E-mail: rgreen@noao.edu
Received 1993 December 27; accepted 1994 April 11

ABSTRACT

We have combined low-dispersion *International Ultraviolet Explorer* (*IUE*) spectra with the optical/near-IR spectrophotometry of Neugebauer et al. (1987) in order to study the spectral energy distributions of seven of the brightest Palomar-Green quasars at intermediate redshifts ($0.9 \leq z_{em} \leq 1.5$). Some of these PG quasars are barely detectable in long *IUE* exposures, so we have used the Gaussian Extraction (GEX) technique to maximize the signal-to-noise of the *IUE* data, and we have co-added all spectra available from the *IUE* archive for each QSO unless the ultraviolet spectra varied significantly from one exposure to the next. We have corrected the spectral energy distributions for Milky Way reddening using the observed neutral hydrogen column densities on each sight line and the gas-to-dust relation recently derived by Diplas & Savage.

Six of the seven quasars are detected down to $\lambda \ll 700$ Å in the rest frame, and consequently continuum reddening due to dust in the immediate vicinity of the quasar can have a dramatic effect on the spectral energy distributions, even if the intrinsic $E(B-V)$ is very small by Galactic standards. In order to explore the possible importance of intrinsic continuum reddening, we have assembled a heuristic extinction curve which extends to $\lambda \ll 912$ Å. Since the 2200 Å bump has never been detected in quasar spectra, longward of the Lyman limit our heuristic extinction curve is based on the Small Magellanic Cloud extinction curve (which contains very little 2200 Å bump). Shortward of the Lyman limit, our extinction curve smoothly increases down to $\lambda \approx 700$ Å ($h\nu \approx 18$ eV) and then turns over in crude accordance with theoretical work based on the Kramers-Kronig relations and laboratory studies. Using this heuristic extinction curve, we derive reasonable upper limits on the intrinsic $E(B-V)$ for each quasar based on the maximum amount of continuum dereddening which can be applied without giving the big blue bump a complex shape. For six out of the seven quasars, we find that the intrinsic $E(B-V) < 0.03$, and the seventh QSO requires intrinsic $E(B-V) < 0.045$. We briefly discuss some of the implications of the derived intrinsic continuum reddening limits.

We use geometrically thin accretion disk models to derive the black hole masses and accretion rates implied by the spectral energy distributions. Even if we neglect intrinsic reddening, we find that a large fraction of the quasars require super-Eddington accretion rates (which is not consistent with the thin disk assumption). Comparison of the data in this paper to a large body of data from the literature on the accretion disk $M_{BH} - \dot{M}$ grid calculated by Wandel & Petrosian reveals that our quasars are among the brightest in the sky at 1450 Å, and ostensibly suggests that the fraction of quasars which require super-Eddington accretion rates is much smaller than the fraction that we derive from our data alone. However, intrinsic continuum reddening has been ignored in this comparison, and a small amount of intrinsic reddening will push more of the quasars into the super-Eddington regime. We also plot the recent reverberation monitoring results on NGC 5548 and NGC 3783 on the Wandel & Petrosian grid, and we find that these Seyfert galaxies appear to vary along lines of constant M_{BH}.

Continuum flux from two of the quasars in our main sample, PG 1338+416 and PG 1630+377, is detected at $\lambda_{rest} < 584$ Å. These quasars can in principle be used for the He I Gunn-Peterson test, but the S/N of *IUE* spectra of individual objects is usually too low to place interesting limits on the Gunn-Peterson optical depth. In order to improve the S/N, we have formed a composite spectrum from the spectra of five quasars detected with *IUE* at $\lambda_{rest} < 584$ Å, and we have used this composite spectrum to place a tighter limit on $\tau_{GP,He\,I}$. From the composite spectrum we find that at $\langle z_{em} \rangle = 1.58$, $\tau_{GP,He\,I} \leq 0.09$ at the 3 σ level.

[1] Guest Observer with the *International Ultraviolet Explorer* satellite, sponsored and operated by the National Aeronautics and Space Administration (USA), the Science and Engineering Council (UK), and the European Space Agency.

[2] The National Optical Astronomy Observatories are operated by the Association of Universities for Research in Astronomy, Inc. (AURA), under cooperative agreement with the National Science Foundation.

We briefly discuss intermediate-redshift Lyman limit systems ($0.5 \leq z_{LL} \leq 1.6$) detected in the *IUE* spectra of five quasars, including lower limits on N(H I) in each Lyman limit system.

Subject headings: accretion, accretion disks — dust, extinction — infrared: galaxies — intergalactic medium — quasars: general — ultraviolet: galaxies

1. INTRODUCTION

Perhaps the most popular of the various quasar puzzles is the question of the central engine. How can so much luminosity originate in such a small region of space? An extensive amount of literature has been devoted to the subject, and the general assumption is that quasars and other forms of active galactic nuclei (AGNs) are powered by gravitational energy released during the accretion of matter onto a black hole (e.g., Salpeter 1964; Lynden-Bell 1969). The black hole accretion disk model has been invoked to explain the shape of a portion of the continuum energy distribution, the so-called "big blue bump" extending from the optical into the ultraviolet. This big blue bump, which is defined as the optical/UV excess above an underlying IR/X-ray power law, was first modeled with an accretion disk by Shields (1978), and Malkan (1983) has shown that observed AGN spectra can be successfully fitted by treating the accretion disk as concentric blackbodies at high temperatures near the inner edge and decreasing temperatures at larger radii. Since then, increasingly sophisticated accretion disk models have been calculated including, for example, the effects of electron scattering and Comptonization (Czerny & Elvis 1987; Wandel & Petrosian 1988), use of stellar atmospheres instead of blackbodies to approximate the local disk spectrum (Kolykhalov & Sunyaev 1984; Sun & Malkan 1987), and relativistic and inclination effects (Sun & Malkan 1989; Laor & Netzer 1989). More recent calculations have also considered the continuous emission produced by accretion disks around rotating as well as nonrotating black holes (Sun & Malkan 1989; Laor 1990; Wandel 1991), and Field & Rogers (1993) have calculated the spectrum emitted by an AGN accretion disk that contains magnetic fields.

There are some observational problems with the black hole accretion disk paradigm (see Malkan 1992; Kinney 1994), and some alternatives to the accretion disk model of the big blue bump have been hypothesized. One of the earliest alternatives suggested was that the optical/UV continuum is generated by synchrotron emission and Compton scattering (Jones, O'Dell, & Stein 1974a, b; Puetter et al. 1982; O'Dell, Scott, & Stein 1987; Jones & Stein 1987). Several authors have proposed that the big blue bump is thermal (free-free) emission that originates in a hot optically thin gas with a large covering factor (Malkan & Sargent 1982; Antonucci & Barvainis 1988; Malkan 1989; Ferland, Korista, & Peterson 1990; Barvainis 1993). A third possibility put forth by Lightman & White (1988), Guilbert & Rees (1988), and Ferland & Rees (1988) is that the big blue bump is reprocessed emission from a spherical shell of dense cold clouds that absorb the AGN X-ray continuum and reemit it in the optical and ultraviolet. Reprocessing also played an important role in the early model of Daltabuit, MacAlpine, & Cox (1978) which showed that various features of quasar spectra could be produced by collisions of very high velocity clouds.

Of course, observations constrain the models. Hopefully, the models will eventually become sufficiently refined and the observations sufficiently extensive so that the most appropriate model can be identified. Spectrophotometry is required because the models are constrained by the luminosity as well as the shape of the big blue bump, and therefore absolute fluxes are needed (and results are sensitive to uncertainties in the cosmological parameters). Neugebauer et al. (1987) have provided nearly simultaneous spectrophotometric optical and infrared observations of 105 quasars in the Palomar-Green survey (Green, Schmidt, & Liebert 1986; Schmidt & Green 1983). Since the ultraviolet continuum is a critical region of the spectrum for big blue bump studies, we have used the *International Ultraviolet Explorer Satellite* (*IUE*) to extend the Neugebauer et al. (1987) spectral energy distributions of seven of the brightest intermediate-redshift PG quasars well into the rest frame ultraviolet, and we present the resultant infrared to ultraviolet spectral energy distributions in this paper. When we started this program, *IUE* was the only telescope available for ultraviolet spectrophotometry. The data are still of considerable value, because the absolute flux calibration of low-dispersion *IUE* spectra obtained with the large aperture is well-established and stable (Bohlin et al. 1990 and references therein). The seven quasars that we concentrate on in this paper are the brightest intermediate-redshift Palomar-Green quasars that are not included in the samples of Green et al. (1980) or Bechtold et al. (1984). The average redshift of the seven quasars is 1.2. Ironically, while the average redshift of the QSOs observed by Bechtold et al. (1984) is 1.5, on average we see farther into the rest frame UV in the sample in this paper than in the Bechtold et al. (1984) sample because intervening optically thick Lyman limits more frequently obliterate the UV spectra of higher redshift objects.

The paper is organized as follows. In § 2 we review the *IUE* observations and data reduction. In § 3 we present the observed spectral energy distributions. Laor (1990) has shown that intrinsic reddening by dust in the host galaxy of a quasar can dramatically affect accretion disk models fit to the object's continuum, so in § 4 we employ a hypothetical extinction curve, which extends below the Lyman limit, in order to explore the possible effects of intrinsic reddening on QSO continua. In § 5 we discuss accretion disk models; we use a simple geometrically thin accretion disk model to derive the black hole masses and accretion rates required for the objects presented in this study. We find that this model requires super-Eddington accretion rates for a substantial portion of our sample, so we also compare the observations to the more sophisticated accretion disk models of Wandel & Petrosian (1988) which include electron scattering and Comptonization and are less likely to require supercritical accretion rates. In § 6 we discuss some effects of intergalactic absorption on the spectral energy distributions. We use five quasars detected below 584 Å in the rest frame to build a composite spectrum which we use to carry out an improved He I Gunn-Peterson test, and we briefly discuss low-redshift Lyman limits. In § 7 we summarize the paper.

2. *IUE* OBSERVATIONS AND DATA REDUCTION

The ultraviolet spectra were obtained with the *IUE* by blind offset of the targets into the large (10″ × 20″) aperture. The blind offset technique was used to center the targets in the aperture because the quasars are too faint to be detected in the

normal operation of the photoelectric fine error sensor. A log of the *IUE* observations is given in Table 1. Table 1 also lists the visual magnitudes and redshifts of the quasars we have observed (from Hewitt & Burbidge 1987) and the column density of Galactic neutral hydrogen on each sight line (from Elvis, Lockman, & Wilkes 1989 or Stark et al. 1992).

We have extracted the *IUE* spectra using the Gaussian Extraction technique (GEX) developed by Urry & Reichert (1988). In detailed comparisons of the standard IUESIPS extraction to GEX and the "optimal" extraction technique (which is described by Kinney, Bohlin, & Neill 1991), Kinney, Bohlin, & Neill (1988, 1990) find that both GEX and the optimal extraction technique significantly improve the signal-to-noise ratio (S/N) of spectra taken at low net signal levels while conserving total flux (the standard line-by-line extraction using a narrow slit provides a comparable improvement of the S/N but loses a small amount of flux). Kinney et al. (1990) also find that "because GEX assumes that the cross-dispersion profile is Gaussian in shape, GEX can handle low level detections better than the weighted polynomial slit extraction." However, GEX can only be used to reduce point source spectra. The intermediate-redshift PG QSOs in this paper are just above the *IUE* low-level detectability limits; consequently, we have chosen GEX in order to maximize the S/N. The standard *IUE* absolute flux calibration was applied to each spectrum.

Most of the quasars in Table 1 have been observed more than once during the lifetime of the *IUE*, and some of the observations are separated by a few years. Since the ultraviolet fluxes of many QSOs are variable, one cannot blindly co-add all observations available from the *IUE* archives. We have extracted all individual observations of each quasar. Before co-adding the data, we have compared the individual spectra of a given object to each other, and if they are not significantly different, we have combined them, weighted by the exposure time, using the IRAF[3] avsigclip algorithm. If instead the individual spectra turn out to be different from each other, we have used only the pair of short and long wavelength observations with the least separation in observation date. Thus the *IUE* images listed in Table 1 are not necessarily the only observations available from the *IUE* archives. The co-added and flux-calibrated spectra of the seven PG quasars of primary interest and five additional quasars (which we shall use for the He I Gunn-Peterson test and a brief discussion of intermediate-redshift Lyman limit systems) are shown in Figure 1. Spectra of these objects, reduced with different S/N optimizing algorithms, are also found in Kinney et al. (1991b) and Lanzetta, Turnshek, & Sandoval (1993).

Most *IUE* spectra contain fixed-pattern noise which is due to the misalignment of the observation image with the image transfer function images used for flat-fielding. Long *IUE* exposures of faint objects are prone to a few extra problems. In addition to the usual increase in cosmic-ray hits, *IUE* observa-

[3] IRAF is distributed by NOAO, which is operated by AURA, Inc., under contract to the NSF.

TABLE 1

LOG OF *IUE* OBSERVATIONS

Quasar	z	V[a]	N_{HI}^{b} (10^{20} cm^{-2})	*IUE* Image No.	Observation Date (year,day)	Exposure Duration (minutes)
PG 0117+213	1.493	16.05	4.85	LWP9720	1986,351	405
PHL 1377	1.436	16.46	2.29	SWP16252	1982,034	513
(0232-042)				LWR12023	1981,325	410
Ton 34	1.928	15.69	2.66	SWP28188	1986,108	390
(1017+280)				SWP32375	1987,325	325
				LWP5708	1985,100	430
PG 1148+549	0.969	15.82	1.20	SWP14454	1981,193	200
				LWR11052	1981,193	180
PG 1206+459	1.158	15.79	1.27	SWP19805	1983,114	435
				LWR15796	1983,112	425
PG 1241+176	1.273	15.38	1.93	SWP22338	1984,054	490
				LWP2836	1984,054	300
				LWP6202	1985,164	280
				LWP6215	1985,165	280
				LWP6246	1985,169	300
				LWP6247	1985,170	300
				LWP6262	1985,175	465
PG 1248+401	1.030	16.06	1.49	SWP15535	1981,324	410
PG 1338+416	1.219	16.08	0.96	SWP28205	1986,110	375
				SWP30294	1987,042	325
				SWP30347	1987,051	420
				LWP5713	1985,101	385
PG 1407+265	0.944	15.73	1.38	SWP19858	1983,120	356
				LWP9733	1986,353	400
PG 1522+101	1.321	15.74	2.83	SWP17098	1982,153	357
				SWP19840	1983,118	379
				LWR13008	1982,102	410
PG 1630+377	1.471	15.96	0.90	SWP22440	1984,068	350
				SWP22444	1984,069	354
				SWP33225	1988,098	405
				LWP4265	1984,265	435
PG 1715+535	1.920	16.30	2.68	LWP10151	1987,050	410

[a] From Hewitt & Burbidge 1987.
[b] From Stark et al. 1992 or Elvis, Lockman, & Wilkes 1989.

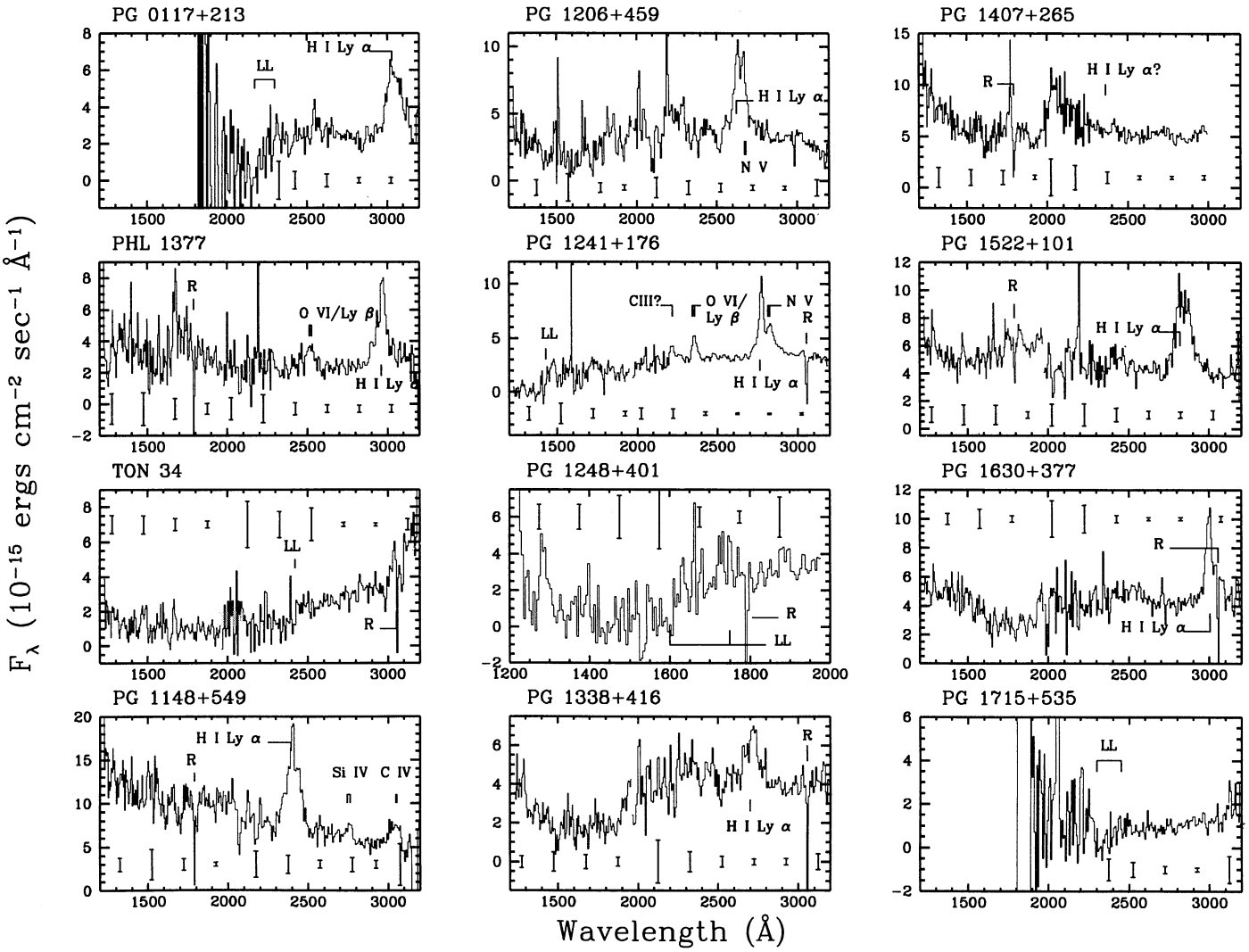

FIG. 1.—*IUE* spectra of 10 Palomar-Green quasars and two additional quasars which are useful for the He I Gunn-Peterson test. The spectra have been extracted with the Gaussian Extraction Software (GEX) and co-added as described in the text. Sample error bars are shown in each panel, and pixels adversely affected by reseaux are indicated by an R. Lyman limits (LL) and emission-line identifications are also indicated.

tions of faint sources with the short-wavelength prime (SWP) camera have been shown to suffer a continuum distortion which produces a flux deficit near 1650 Å and a flux excess near 1500 Å (Hackney, Hackney, & Kondo 1982). Finley, Basri, & Bowyer (1990) have derived a flux calibration correction for this problem based on observations of hot DA white dwarfs, but since the amplitude of the distortion appears to increase with decreasing source intensity (i.e., longer exposure duration), this correction sometimes is not adequate for *IUE* QSO spectra. Also, camera artifacts that resemble emission features recur in long-duration exposures at particular wavelengths but are not detectable in short-exposure spectra (Hackney et al. 1982). These exposure-dependent artificial emission features have been identified using sky background observations by Crenshaw, Bruegman, & Norman (1990).

GEX fits a linear background plus a Gaussian to the signal perpendicular to the dispersion direction. The fitted linear background in a given region of the detector is a relatively smoothly changing function of wavelength, and the background is the dominant source of noise in the gross signal. In order to estimate the flux uncertainties, we have used the *IUE* RDAF task EXESLO to extract the signal from a number (equal to the full width at half-maximum of the fitted Gaussian) of consecutive lines in the background region of the detector, and we have used the fluctuations of this background signal about the GEX linear background fit to estimate the flux uncertainties. Sample error bars estimated in this way are shown in Figure 1.

3. SPECTRAL ENERGY DISTRIBUTIONS

The observed spectral energy distributions are tabulated in Table 2. No corrections for Galactic or intrinsic reddening have been applied to the data in Table 2. The optical observations were made from one to several years before the ultraviolet observations; consequently, in some cases there is a discontinuity between the optical and ultraviolet spectra due to mild variability of the QSO. In order to obtain uniform spectral energy distributions, we have "grayshifted" some of the spectra (as indicated in Table 2) by a small amount to remove the discontinuity. Since O'Brien, Gondhalekar, & Wilson (1988a) find that the *shape* of the continuum of a variable quasar usually does not change even though the level does

TABLE 2

OBSERVED SPECTRAL ENERGY DISTRIBUTIONS[a]

QSO= log ν	PG 0117+213	PG 1148+549	PG 1206+459[b]	PG 1241+176	PG 1338+416[c]	PG 1407+265[d]	PG 1630+377[e]
			log F_ν (ergs s^{-1} cm^{-2} Hz^{-1})				
15.371	...	-26.15±.04	-26.70±.10	...	...	-26.33±.03	...
15.355	...	-26.14±.03	-26.82±.32	...	...	-26.35±.06	...
15.339	...	-26.11±.24	-26.74±.09	...	-26.89±.07	-26.35±.06	-26.45±.03
15.323	...	-26.14±.06	-26.93±.25	...	-26.89±.12	-26.38±.09	-26.46±.05
15.308	...	-26.10±.04	-26.72±.11	-26.78±.13	-27.01±.13	-26.40±.06	-26.46±.05
15.294	...	-26.03±.06	-26.67±.31	-26.97±.36	-26.98±.18	-26.39±.06	-26.51±.08
15.280	...	-26.05±.05	-26.93±.40	-26.55±.17	-26.83±.22	-26.28±.06	-26.45±.07
15.266	...	-26.08±.04	-26.96±.36	-27.05±.48	-26.88±.10	-26.44±.06	-26.61±.07
15.253	...	-26.05±.04	-26.56±.07	-26.84±.22	-26.97±.12	-26.32±.07	-26.58±.07
15.240	...	-26.02±.03	-26.79±.10	-26.58±.07	-26.79±.06	-26.25±.05	-26.53±.05
15.228	...	-26.04±.03	-26.60±.07	-26.70±.08	-26.81±.05	-26.16±.02	-26.60±.04
15.216	...	-25.96±.02	-26.36±.03	-26.62±.09	-26.75±.10	-26.21±.04	-26.51±.02
15.204	...	-25.92±.01	-26.41±.04	-26.72±.08	-26.83±.05	-26.22±.02	-26.49±.02
15.192	...	-25.91±.01	-26.48±.03	-26.67±.05	-26.51±.02	-26.28±.02	-26.38±.02
15.170	...	-25.84±.07	-26.16±.08	-26.43±.08	-26.36±.13	-26.20±.09	-26.46±.14
15.160	...	-26.00±.06	-26.38±.06	-26.39±.08	-26.31±.12	-26.20±.06	-26.39±.08
15.149	...	-25.88±.08	-26.37±.12	-26.29±.05	-26.31±.12	-26.24±.08	-26.41±.15
15.139	...	-25.92±.09	-26.00±.03	-26.33±.07	-26.31±.12	-26.28±.08	-26.40±.12
15.130	...	-25.87±.06	-26.08±.05	-26.19±.05	-26.29±.09	-26.28±.07	-26.40±.11
15.120	-26.44±.17	-25.92±.07	-26.05±.06	-26.27±.05	-26.16±.05	-26.28±.06	-26.30±.08
15.110	-26.32±.18	-25.77±.05	-26.22±.07	-26.23±.04	-26.14±.04	-26.28±.05	-26.28±.07
15.101	-26.43±.15	-25.60±.03	-26.22±.09	-26.12±.02	-26.19±.06	-26.29±.04	-26.30±.04
15.092	-26.34±.09	-25.52±.03	-26.11±.04	-26.22±.02	-26.14±.04	-26.24±.03	-26.21±.02
15.083	-26.32±.06	-25.72±.02	-26.13±.04	-26.19±.02	-26.12±.02	-26.28±.03	-26.20±.02
15.075	-26.20±.03	-25.85±.05	-26.21±.05	-26.18±.02	-26.20±.03	-26.27±.05	-26.16±.02
15.066	-26.20±.05	-25.80±.03	-26.00±.02	-26.19±.01	-26.10±.02	-26.26±.02	-26.16±.01
15.058	-26.22±.06	-25.83±.03	-25.71±.03	-26.16±.01	-26.10±.01	-26.24±.02	-26.20±.01
15.050	-26.19±.02	-25.81±.02	-25.73±.01	-26.13±.01	-25.96±.01	-26.19±.01	-26.20±.01
15.041	-26.23±.03	-25.80±.02	-25.97±.02	-26.01±.01	-25.89±.01	-26.17±.01	-26.16±.02
15.034	-26.20±.02	-25.76±.05	-26.02±.02	-25.71±.01	-25.99±.01	-26.20±.01	-26.18±.01
15.026	-26.26±.03	-25.83±.03	-26.03±.02	-25.82±.01	-26.08±.01	-26.18±.01	-26.16±.01
15.018	-26.17±.02	-25.82±.03	-26.06±.04	-25.92±.01	-26.05±.02	-26.20±.01	-26.12±.01
15.011	-26.12±.03	-25.82±.04	-26.04±.02	-25.99±.01	-26.08±.02	-26.13±.01	-26.09±.01
15.003	-25.98±.03	-25.76±.06	-26.07±.04	-25.99±.01	-26.04±.02	-26.08±.02	-25.86±.01
14.996	-25.75±.01	-25.66±.04	-25.98±.05	-25.98±.01	-26.01±.02	-26.00±.01	-25.83±.01
14.989	-25.78±.06	-25.70±.17	-26.07±.05	-26.17±.02	-26.12±.04	...	-26.06±.02
14.982	-25.93±.05	-25.81±.10	-26.10±.11	-25.97±.02	-25.96±.04	...	-26.04±.04
14.975	-26.06±.11	...	-26.18±.16	...	-25.95±.06	...	-25.99±.05
14.969	-26.04±.03	...	-26.07±.04	...	-25.94±.06	-26.20±.08	-26.02±.07
14.959	-26.05±.03	-25.79±.04	...	-25.96±.04	-25.90±.05	-26.14±.05	-25.95±.05
14.948	-26.06±.02	-25.77±.02	...	-25.96±.03	...	-26.15±.03	-25.97±.02
14.938	...	-25.79±.02	-26.06±.02	...	...	-26.13±.03	...
14.928	...	-25.76±.01	...	...	...	-26.16±.02	-26.00±.02
14.918	-26.10±.02	-25.75±.02	-26.07±.02	...	...	...	-26.00±.03
14.909	-26.03±.02	...	-26.07±.01	...	-25.95±.02	...	-25.94±.02
14.900	...	...	...	...	-25.98±.07	...	...
14.891	...	...	-26.04±.01	-25.90±.02	-25.96±.02	-26.15±.02	...
14.882	...	-25.77±.01	-26.02±.01	-25.93±.02	-25.95±.02	-26.16±.02	...
14.873	-25.99±.01	-25.75±.01	...	-25.87±.01	-25.93±.02	-26.10±.02	...
14.864	...	-25.73±.01	...	-25.87±.01	...	-26.10±.02	-25.94±.02
14.856	-25.98±.01	-25.75±.01	...	-25.86±.01	...	-26.08±.01	-25.97±.01
14.848	-25.98±.01	-25.76±.01	...	...	...	-26.12±.02	-25.96±.02
14.840	-25.99±.01	-25.78±.01	-26.01±.01	...	...	-26.13±.01	-25.96±.01
14.832	-25.99±.01	-25.76±.01	-25.97±.01	...	-25.95±.02	-26.08±.02	-25.97±.02
14.824	-25.96±.01	-25.74±.01	-25.96±.01	-25.85±.01	-25.93±.01	-26.06±.01	-25.96±.01
14.816	-25.97±.01	-25.70±.01	-25.98±.01	-25.84±.02	-25.96±.02	-26.06±.02	...
14.809	...	-25.72±.01	-25.98±.01	-25.84±.01	-25.91±.02	-26.04±.02	...
14.801	...	-25.70±.01	-25.98±.01	-25.83±.02	-25.97±.02	-26.05±.02	...
14.794	...	-25.67±.01	-25.97±.01	-25.82±.01	-25.93±.02	-26.05±.01	...
14.787	...	-25.66±.01	-25.98±.01	-25.81±.02	-25.94±.02	-26.05±.02	-25.96±.02
14.780	-25.95±.01	-25.67±.01	-25.93±.01	-25.82±.01	-25.94±.02	-26.04±.01	-25.99±.02
14.773	-25.94±.01	-25.67±.01	-25.91±.01	-25.80±.02	-25.92±.02	-26.04±.02	-25.90±.02
14.766	-25.92±.01	-25.68±.01	-25.90±.01	-25.79±.01	-25.89±.02	-26.04±.02	-25.92±.02
14.759	-25.89±.02	-25.68±.01	-25.87±.01	-25.79±.02	-25.90±.02	-26.04±.02	-25.93±.02

TABLE 2—*Continued*

QSO= log ν	PG 0117+213	PG 1148+549	PG 1206+459	PG 1241+176	PG 1338+416	PG 1407+265	PG 1630+377
			log F_ν (ergs s^{-1} cm^{-2} Hz^{-1})				
14.753	-25.92±.01	-25.70±.01	-25.87±.01	-25.75±.01	-25.93±.02	...	-25.94±.02
14.746	-25.91±.01	...	-25.88±.01	-25.77±.02	-25.85±.02	...	-25.94±.02
14.740	-25.91±.01	...	-25.87±.01	-25.75±.01	-25.88±.02	...	-25.91±.02
14.734	-25.88±.02	...	-25.87±.02	-25.75±.02	-25.89±.03	...	-25.89±.03
14.727	-25.91±.02	...	-25.89±.01	-25.75±.02	-25.87±.02	...	-25.94±.02
14.721	-25.91±.02	...	-25.89±.02	-25.73±.02	-25.93±.02	-26.02±.02	-25.91±.02
14.715	-25.86±.02	-25.67±.02	-25.90±.02	-25.73±.02	-25.92±.03	-26.01±.02	-25.86±.03
14.711	-25.89±.01	-25.69±.01	...	-25.77±.02	-25.95±.02	-26.08±.02	-25.93±.02
14.699	-25.90±.01	-25.74±.01	...	-25.74±.01	...	-26.07±.02	-25.92±.02
14.688	-25.83±.01	-25.68±.01	...	...	...	-26.02±.01	-25.87±.01
14.676	-25.80±.01	-25.63±.01	-25.80±.01	...	...	-26.00±.02	-25.85±.02
14.666	-25.81±.01	-25.64±.01	-25.82±.01	...	-25.84±.01	-26.04±.01	-25.86±.01
14.655	-25.83±.01	-25.66±.01	-25.86±.01	-25.68±.01	-25.87±.02	-26.03±.02	-25.86±.02
14.645	...	-25.66±.01	-25.84±.01	-25.68±.01	-25.87±.02	-26.06±.02	...
14.635	...	-25.64±.02	-25.81±.01	-25.69±.02	-25.86±.02	-26.06±.02	...
14.625	...	-25.65±.01	-25.80±.01	-25.67±.01	-25.81±.01	-26.05±.02	...
14.615	-25.75±.01	-25.65±.02	-25.82±.01	-25.66±.02	-25.86±.02	-26.05±.02	-25.84±.02
14.606	-25.75±.01	-25.65±.01	-25.80±.01	-25.65±.01	-25.85±.01	-26.06±.02	-25.83±.01
14.596	-25.75±.02	...	-25.77±.02	-25.63±.02	-25.82±.02	...	-25.84±.02
14.587	-25.78±.02	...	-25.84±.02	-25.65±.02	-25.82±.03	...	-25.86±.03
14.578	-25.77±.02	-25.69±.02	-25.84±.02	-25.66±.03	-25.81±.03	...	-25.80±.02
14.570	-25.79±.02	...	-25.85±.02	-25.64±.02	-25.83±.03	-26.06±.03	-25.77±.02
14.561	-25.72±.02	-25.66±.03	-25.84±.03	-25.66±.03	-25.88±.04	-26.02±.03	-25.82±.03
14.373	-25.78±.04	-25.52±.04	-25.86±.03	-25.47±.03	-25.99±.04	-26.08±.05	-25.85±.06
14.260	-25.73±.04	-25.58±.02	-25.83±.03	-25.43±.04	-25.91±.02	-26.06±.03	-25.78±.05
14.129	-25.73±.02	-25.43±.02	-25.73±.02	-25.35±.04	-25.87±.02	-26.09±.04	-25.77±.03
13.909	-25.48±.08	...	...	...	...	...	<-25.56
13.473	-24.67±.14	...	...	...	...	...	<-24.29

a All quantitites are in the observer's frame, and no reddening corrections have been applied. A small amount of grayshifting was applied as indicated below.

[b] PG 1206+459 optical spectrum grayshifted by $\Delta \log F_\nu = -0.2$.

[c] PG 1338+416 SWP and LWP spectra grayshifted by $\Delta \log F_\nu = -0.1$.

[d] PG 1407+265 optical and LWP spectra grayshifted by $\Delta \log F_\nu = -0.3$.

[e] PG 1630+377 LWP spectrum grayshifted by $\Delta \log F_\nu = -0.2$.

(however, see Cutri et al. 1985 and the discussion of the Seyfert galaxies NGC 5548 and NGC 3783 in § 5), we have simply applied a small shift to the flux level of the brighter spectrum in cases where there is a discontinuity.

Milky Way reddening was removed using the R_V-dependent extinction curve of Cardelli, Clayton, & Mathis (1989). Preliminary results of a study of ultraviolet Galactic extinction toward distant and moderately reddened giant and supergiant O9–B2 stars (Cardelli & Sembach 1992) show that ultraviolet extinction on low-density sight lines is well characterized by the Cardelli, Clayton, & Mathis (1989) extinction curve with $R_V[\equiv A_V/E(B-V)] = 2.6$–3.4. We have therefore assumed that $\langle R_V \rangle = 3.0$ in order to correct our QSO spectra for Galactic reddening. We have estimated the Galactic color excess using the observed H I column densities on each sight line from Elvis et al. (1989) or Stark et al. (1992; see Table 1) and the atomic hydrogen to color excess relation derived by Diplas & Savage (1994a, b) from interstellar Lyα absorption observed with *IUE* toward late O and early B stars. Based on the 200 sight lines in their sample with E(Bump) measurements (i.e., measurements of the strength of the extinction bump; see Savage et al. 1985), Diplas & Savage (1994b) obtain

$$\frac{N(\mathrm{H\ I})}{E(B-V)} = 4.77 \times 10^{21} \text{ atoms cm}^{-2} \text{ mag}^{-1} . \quad (1)$$

This is the relation we have employed for our Galactic reddening corrections. The spectral energy distributions, corrected for Galactic reddening and grayshifted, are plotted in Figure 2 and tabulated in Table 3.

As noted in § 1, the spectral energy distributions of the seven QSOs in this sample are detected farther into the UV, on average, than in the sample studied by Bechtold et al. (1984). This is due to the increasing probability of intersecting an optically thick Lyman limit system with increasing redshift (Lanzetta 1991, and references therein). In fact, the four quasars in the Bechtold et al. (1984) sample with $1.9 \leq z_{\rm em} \leq 2.2$ are detected, on average, down to 727 Å in the rest frame while the 12 quasars with $0.94 < z_{\rm em} < 1.9$ in this paper combined with the rest of the Bechtold et al. (1984) sample are detected down to 666 Å on average. Therefore further space-based observations of the EUV portion of the big blue bump may be more successful with intermediate-redshift samples than with high-redshift samples.

3.1. *Comments on Individual Objects*

PG 1407+265.—The broad and strong H I Lyα emission line characteristic of quasars is evidently missing from the spectrum of PG 1407+265 (see Figs. 1 and 2). This object may be a misidentified lower redshift BL Lac object. PG 1407+265 has been observed with the *Hubble Space Telescope* (*HST*) Faint Object Spectrograph (FOS) as part of the Quasar Absorption Line Key Project (Bahcall et al. 1993; Schneider et al. 1993), and the Lyα emission line is also missing from the FOS spectrum. The broad noisy feature in the *IUE* spectrum at ~2050 Å is an *IUE* artifact; the sensitivity of the *IUE* long-wavelength prime camera is poor near 2000 Å, and this feature is not present in the *HST* spectrum.

PG 1206+459, PG 1338+416, and PG 1630+377.—The

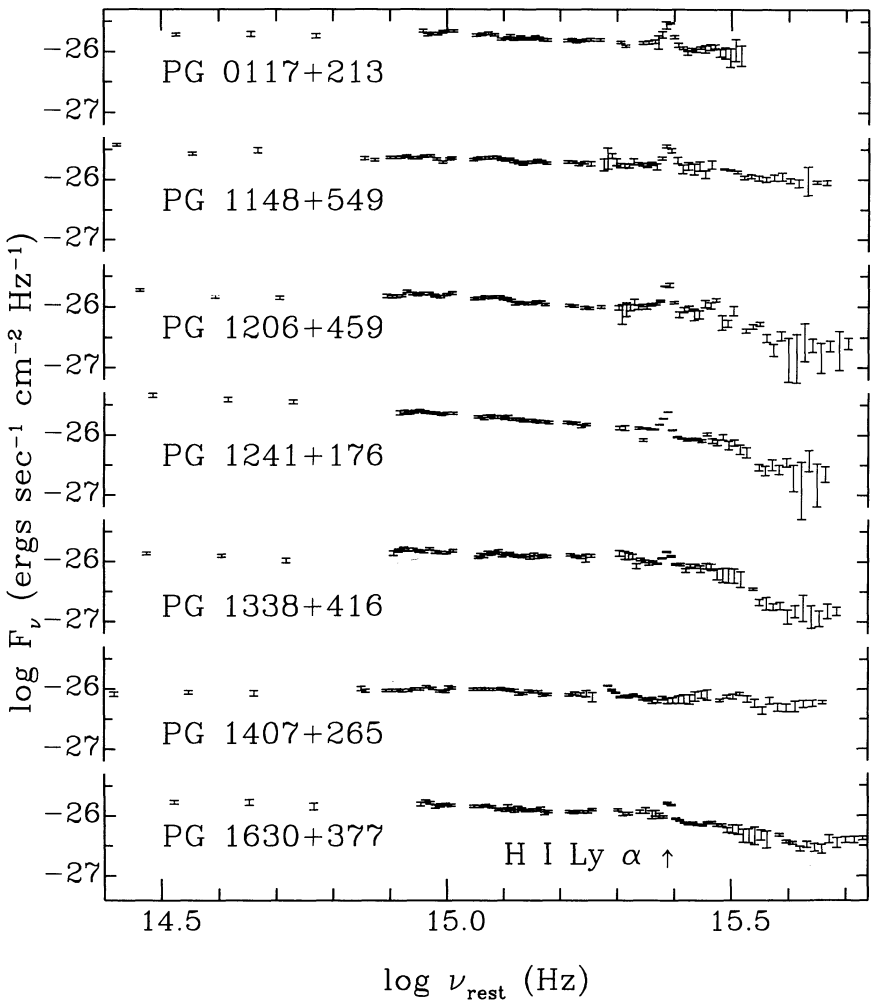

FIG. 2.—Spectral energy distributions of seven PG quasars. These are the brightest PG quasars at intermediate redshifts that were not included in the samples of Green et al. (1980) or Bechtold et al. (1984). The optical/IR data are from Neugebauer et al. (1987), and the UV data are from the *IUE* observations summarized in Table 1. The data have been corrected for Milky Way reddening, but no corrections for intrinsic reddening have been applied. Slight grayshifts have been applied to some of the spectra as indicated in Table 2. The spectral energy distributions plotted in this figure are tabulated in Table 3.

HST Key Project has obtained spectra of PG 1206+459 and PG 1338+416 as well (see Bahcall et al. 1993), and these spectra compare well with the *IUE* spectra shown in Figure 1. The SWP spectra of PG 1206+459, PG 1338+416, and PG 1630+377 contain broad dips with minima at ~730 Å in the rest frame. These dips are not likely to be the "Lyman valley" discussed by Møller & Jakobsen (1990), but they could be Lyman limits (see § 6.2).

Ton 34.—The continuum flux from Ton 34 is marginally detected blueward of the Lyman limit at $z_{LL} = 1.6$. The observed flux level in the Ton 34 SWP spectra ($F_\lambda \approx 1 \times 10^{-15}$ ergs cm^{-2} s^{-1} Å^{-1}; see Fig. 1) is comparable to the residual phosphorescence level in *IUE* images taken after heavy over exposures (Snijders 1983; Imhoff 1987), so the apparent SWP continuum could be an instrument artifact. However, the two SWP observations of Ton 34 made more than a year apart (Table 1) both show continuum emission at this low level, and both SWP spectra connect smoothly to the long-wavelength spectrum (LWP 5708) obtained at least a year before the SWP observations. Therefore we conclude that this continuum flux is probably real, and Ton 34 is a good target for UV *HST* observations.

4. INTRINSIC REDDENING

A difficult and possibly critical issue that must be considered in studies of quasar spectral energy distributions is the amount and effect of intrinsic reddening by dust in the immediate vicinity of quasars, reddening by intergalactic dust, and reddening by dust in intervening objects that intercept the line of sight. This is a difficult issue because continuum emission from many quasars is detected at rest wavelengths well blueward of the Lyman limit (see §§ 3, 6.1), but the properties of dust and the extinction curve below 912 Å are not well known. The properties of dust below the Lyman limit have been theoretically explored (e.g., Draine & Lee 1984; Mathis 1986; Martin & Rouleau 1991; Hawkins & Wright 1991; Laor & Draine 1993), but the extinction curve below the Lyman limit has not been empirically determined due to the obvious problem with the opacity of the interstellar medium at $\lambda \leq 912$ Å. Furthermore, in addition to the R_V dependence noted by Cardelli et al. (1989), extinction curves are known to be significantly different in different environments found in the Milky Way ISM (Cardelli & Clayton 1991; Mathis & Cardelli 1992 and references therein) and in different galaxies (Fitzpatrick 1989 and

TABLE 3

OBSERVED SPECTRAL ENERGY DISTRIBUTIONS CORRECTED FOR GALACTIC REDDENING[a]

QSO=	PG 0117+213	PG 1148+549	PG 1206+459[b]	PG 1241+176	PG 1338+416[c]	PG 1407+265[d]	PG 1630+377[e]
log ν			log F_ν (ergs s^{-1} cm^{-2} Hz^{-1})				
15.371	...	-26.05±.04	-26.60±.10	...	...	-26.22±.03	...
15.355	...	-26.04±.03	-26.72±.32	...	...	-26.24±.06	...
15.339	...	-26.02±.24	-26.64±.09	...	-26.82±.07	-26.24±.06	-26.38±.03
15.323	...	-26.06±.06	-26.84±.25	...	-26.82±.12	-26.28±.09	-26.40±.05
15.308	...	-26.01±.04	-26.63±.11	-26.65±.13	-26.94±.13	-26.31±.06	-26.40±.05
15.294	...	-25.95±.06	-26.58±.31	-26.83±.36	-26.91±.18	-26.30±.06	-26.45±.08
15.280	...	-25.97±.05	-26.84±.40	-26.42±.17	-26.77±.22	-26.19±.06	-26.39±.07
15.266	...	-26.00±.04	-26.87±.36	-26.92±.48	-26.82±.10	-26.35±.06	-26.55±.07
15.253	...	-25.97±.04	-26.48±.07	-26.72±.22	-26.91±.12	-26.23±.07	-26.53±.07
15.240	...	-25.94±.03	-26.71±.10	-26.45±.07	-26.73±.06	-26.16±.05	-26.47±.05
15.228	...	-25.96±.03	-26.51±.07	-26.57±.08	-26.75±.05	-26.07±.02	-26.54±.04
15.216	...	-25.88±.02	-26.28±.03	-26.50±.09	-26.69±.10	-26.12±.04	-26.45±.02
15.204	...	-25.84±.01	-26.32±.04	-26.59±.08	-26.77±.05	-26.13±.02	-26.43±.02
15.192	...	-25.82±.01	-26.39±.03	-26.53±.05	-26.45±.02	-26.18±.02	-26.32±.02
15.170	...	-25.75±.07	-26.07±.08	-26.29±.08	-26.29±.13	-26.10±.09	-26.39±.14
15.160	...	-25.91±.06	-26.28±.06	-26.24±.08	-26.24±.12	-26.09±.06	-26.32±.08
15.149	...	-25.78±.08	-26.27±.12	-26.13±.05	-26.23±.12	-26.12±.08	-26.33±.15
15.139	...	-25.83±.09	-25.89±.03	-26.17±.07	-26.23±.12	-26.17±.08	-26.33±.12
15.130	...	-25.78±.06	-25.98±.05	-26.04±.05	-26.21±.09	-26.16±.07	-26.33±.11
15.120	-26.07±.17	-25.83±.07	-25.95±.06	-26.12±.05	-26.09±.05	-26.18±.06	-26.23±.08
15.110	-25.97±.18	-25.68±.05	-26.13±.07	-26.09±.04	-26.07±.04	-26.19±.05	-26.22±.07
15.101	-26.10±.15	-25.52±.03	-26.13±.09	-25.98±.02	-26.12±.06	-26.19±.04	-26.24±.04
15.092	-26.03±.09	-25.44±.03	-26.03±.04	-26.10±.02	-26.07±.04	-26.15±.03	-26.16±.02
15.083	-26.02±.06	-25.65±.02	-26.05±.04	-26.07±.02	-26.07±.02	-26.20±.03	-26.15±.02
15.075	-25.91±.03	-25.78±.05	-26.13±.05	-26.07±.02	-26.15±.03	-26.19±.05	-26.11±.02
15.066	-25.92±.05	-25.73±.03	-25.93±.02	-26.08±.01	-26.05±.02	-26.18±.02	-26.11±.01
15.058	-25.95±.06	-25.76±.03	-25.64±.03	-26.05±.01	-26.04±.01	-26.16±.02	-26.16±.01
15.050	-25.93±.02	-25.75±.02	-25.66±.01	-26.03±.01	-25.91±.01	-26.12±.01	-26.15±.01
15.041	-25.98±.03	-25.73±.02	-25.90±.02	-25.91±.01	-25.84±.01	-26.09±.01	-26.12±.02
15.034	-25.96±.02	-25.70±.05	-25.95±.02	-25.61±.01	-25.94±.01	-26.13±.01	-26.13±.01
15.026	-26.02±.03	-25.77±.03	-25.96±.02	-25.72±.01	-26.03±.01	-26.11±.01	-26.11±.01
15.018	-25.94±.02	-25.77±.03	-26.00±.04	-25.82±.01	-26.00±.02	-26.13±.01	-26.08±.01
15.011	-25.89±.03	-25.76±.04	-25.97±.02	-25.90±.01	-26.04±.02	-26.06±.01	-26.04±.01
15.003	-25.76±.03	-25.71±.06	-26.01±.04	-25.90±.01	-25.99±.02	-26.01±.02	-25.82±.01
14.996	-25.53±.01	-25.60±.04	-25.92±.05	-25.89±.01	-25.96±.02	-25.94±.01	-25.79±.01
14.989	-25.56±.06	-25.65±.17	-26.01±.05	-26.08±.02	-26.08±.04	...	-26.01±.02
14.982	-25.71±.05	-25.75±.10	-26.05±.11	-25.88±.02	-25.92±.04	...	-26.00±.04
14.975	-25.84±.11	...	-26.12±.16	...	-25.91±.06	...	-25.95±.05
14.969	-25.83±.03	...	-26.02±.04	...	-25.89±.06	-26.14±.08	-25.98±.07
14.959	-25.85±.03	-25.74±.04	...	-25.88±.04	-25.86±.05	-26.08±.05	-25.91±.05
14.948	-25.85±.02	-25.72±.02	...	-25.88±.03	...	-26.09±.03	-25.93±.02
14.938	...	-25.74±.02	-26.00±.02	...	...	-26.07±.03	...
14.928	...	-25.71±.01	...	...	...	-26.10±.02	-25.96±.02
14.918	-25.91±.02	-25.71±.02	-26.02±.02	...	...	...	-25.97±.03
14.909	-25.85±.02	...	-26.02±.01	...	-25.91±.02	...	-25.90±.02
14.900	...	...	...	...	-25.94±.07	...	...
14.891	...	...	-25.99±.01	-25.82±.02	-25.93±.02	-26.09±.02	...
14.882	...	-25.73±.01	-25.97±.01	-25.85±.02	-25.92±.02	-26.10±.02	...
14.873	-25.81±.01	-25.70±.01	...	-25.80±.01	-25.89±.02	-26.05±.02	...
14.864	...	-25.69±.01	...	-25.80±.01	...	-26.05±.02	-25.90±.02
14.856	-25.80±.01	-25.71±.01	...	-25.79±.01	...	-26.04±.01	-25.94±.01
14.848	-25.81±.01	-25.71±.01	...	...	...	-26.08±.02	-25.93±.02
14.840	-25.82±.01	-25.74±.01	-25.96±.01	...	...	-26.08±.01	-25.93±.01
14.832	-25.83±.01	-25.72±.01	-25.93±.01	...	-25.92±.02	-26.03±.02	-25.94±.02
14.824	-25.80±.01	-25.70±.01	-25.92±.01	-25.79±.01	-25.90±.01	-26.02±.01	-25.93±.01
14.816	-25.82±.01	-25.66±.01	-25.94±.01	-25.78±.02	-25.93±.02	-26.01±.02	...
14.809	...	-25.68±.01	-25.95±.01	-25.78±.01	-25.88±.02	-26.00±.02	...
14.801	...	-25.66±.01	-25.94±.01	-25.77±.02	-25.94±.02	-26.01±.02	...
14.794	...	-25.64±.01	-25.93±.01	-25.76±.01	-25.90±.02	-26.01±.01	...
14.787	...	-25.63±.01	-25.95±.01	-25.76±.02	-25.92±.02	-26.01±.02	-25.93±.02
14.780	-25.81±.01	-25.64±.01	-25.89±.01	-25.76±.01	-25.91±.02	-26.00±.01	-25.96±.02
14.773	-25.80±.01	-25.64±.01	-25.87±.01	-25.74±.02	-25.90±.02	-26.00±.02	-25.88±.02
14.766	-25.78±.01	-25.64±.01	-25.86±.01	-25.74±.01	-25.86±.02	-26.00±.02	-25.90±.02
14.759	-25.76±.02	-25.65±.01	-25.84±.01	-25.74±.02	-25.88±.02	-26.01±.02	-25.90±.02

TABLE 3—*Continued*

QSO= log ν	PG 0117+213	PG 1148+549	PG 1206+459	PG 1241+176	PG 1338+416	PG 1407+265	PG 1630+377
			log F_ν (ergs s^{-1} cm^{-2} Hz^{-1})				
14.753	-25.79±.01	-25.67±.01	-25.84±.01	-25.70±.01	-25.90±.02	...	-25.91±.02
14.746	-25.78±.01	...	-25.85±.01	-25.72±.02	-25.83±.02	...	-25.91±.02
14.740	-25.79±.01	...	-25.84±.01	-25.70±.01	-25.85±.02	...	-25.89±.02
14.734	-25.76±.02	...	-25.84±.02	-25.70±.02	-25.87±.03	...	-25.87±.03
14.727	-25.79±.02	...	-25.86±.01	-25.70±.02	-25.85±.02	...	-25.92±.02
14.721	-25.79±.02	...	-25.86±.02	-25.68±.02	-25.91±.02	-25.99±.02	-25.89±.02
14.715	-25.74±.02	-25.64±.02	-25.87±.02	-25.69±.02	-25.89±.03	-25.97±.02	-25.84±.03
14.711	-25.78±.01	-25.66±.01	...	-25.73±.02	-25.93±.02	-26.04±.02	-25.91±.02
14.699	-25.79±.01	-25.71±.01	...	-25.70±.01	...	-26.04±.02	-25.90±.02
14.688	-25.72±.01	-25.66±.01	...	...	...	-25.99±.01	-25.85±.01
14.676	-25.70±.01	-25.61±.01	-25.78±.01	...	...	-25.97±.02	-25.83±.02
14.666	-25.71±.01	-25.61±.01	-25.80±.01	...	-25.82±.01	-26.01±.01	-25.84±.01
14.655	-25.73±.01	-25.64±.01	-25.83±.01	-25.64±.01	-25.85±.02	-26.01±.02	-25.84±.02
14.645	...	-25.64±.01	-25.81±.01	-25.64±.01	-25.85±.02	-26.03±.02	...
14.635	...	-25.61±.02	-25.78±.01	-25.65±.02	-25.84±.02	-26.03±.02	...
14.625	...	-25.63±.01	-25.78±.01	-25.64±.01	-25.79±.01	-26.02±.02	...
14.615	-25.66±.01	-25.63±.02	-25.80±.01	-25.63±.02	-25.84±.02	-26.03±.02	-25.83±.02
14.606	-25.66±.01	-25.63±.01	-25.78±.01	-25.62±.01	-25.83±.01	-26.03±.02	-25.81±.01
14.596	-25.67±.02	...	-25.75±.02	-25.60±.02	-25.81±.02	...	-25.83±.02
14.587	-25.70±.02	...	-25.82±.02	-25.62±.02	-25.81±.03	...	-25.85±.03
14.578	-25.70±.02	-25.67±.02	-25.82±.02	-25.63±.03	-25.79±.03	...	-25.78±.02
14.570	-25.72±.02	...	-25.83±.02	-25.62±.02	-25.82±.03	-26.04±.03	-25.76±.02
14.561	-25.66±.02	-25.65±.03	-25.82±.03	-25.63±.03	-25.86±.04	-26.00±.03	-25.81±.03
14.373	-25.74±.04	-25.51±.04	-25.85±.03	-25.45±.03	-25.99±.04	-26.07±.05	-25.85±.06
14.260	-25.71±.04	-25.57±.02	-25.83±.03	-25.42±.04	-25.90±.02	-26.05±.03	-25.78±.05
14.129	-25.72±.02	-25.42±.02	-25.73±.02	-25.34±.04	-25.86±.02	-26.09±.04	-25.77±.03
13.909	-25.48±.08	...	...	...	...	...	<-25.56
13.473	-24.67±.14	...	...	...	...	...	<-24.29

a All quantities are in the observer's frame. The fluxes have been corrected for Milky Way reddening, but no intrinsic reddening corrections have been applied. A small amount of grayshifting was applied as indicated below.

[b] PG 1206+459 optical spectrum grayshifted by $\Delta \log F_\nu = -0.2$.

[c] PG 1338+416 SWP and LWP spectra grayshifted by $\Delta \log F_\nu = -0.1$.

[d] PG 1407+265 optical and LWP spectra grayshifted by $\Delta \log F_\nu = -0.3$.

[e] PG 1630+377 LWP spectrum grayshifted by $\Delta \log F_\nu = -0.2$.

references therein), so one cannot blindly apply the Milky Way extinction curve to correct for intrinsic and extragalactic reddening of AGN spectra. In this section we review some of the literature on AGN dust, and we use a heuristic extinction curve, which extends below the Lyman limit, to explore the possible impact of intrinsic reddening on QSO spectral energy distributions.

4.1. *Evidence of Dust in AGN*

Many papers have discussed the use of observed emission-line ratios for the study of dust in AGN. This topic has been reviewed by MacAlpine (1985), and more recent literature is summarized by Netzer & Laor (1993) and Binette et al. (1993). Starting with the Balmer decrement and progressing to other line ratios (e.g., [S II] 4072 Å/[S II] 10320 Å), many authors have found that the observed line ratios are not consistent with simple models and seem to require intrinsic reddening (see MacAlpine 1985). Unfortunately, many line ratios turn out to be sensitive to optical depth effects and physical conditions in the gas, so the amount of intrinsic reddening implied by line ratios is not necessarily easily determined. Probably some dust is present in the narrow-line regions (NLRs) of AGN (MacAlpine 1985; Osterbrock 1989), but the effect of this dust on the spectral energy distribution is uncertain. If the covering factor of the NLR is small, then NLR dust will not significantly affect the spectral energy distribution. Based on their recent radiation transfer calculations, Binette et al. (1993) find that the observed hydrogen line ratios indicate that the covering factor of the NLR is possibly large, so they conclude that intrinsic continuum reddening is important and they explore some of the effects of NLR dust on the continuum.

The absence in quasar spectra of the 2200 Å bump characteristic of the Milky Way extinction curve was initially interpreted to be evidence that dust does not exist in the immediate vicinity of QSOs (McKee & Petrosian 1974). However, it is now known that extinction curves in some galaxies do not contain the 2200 Å bump (e.g., the Small Magellanic Cloud; see Prévot et al. 1984), so this is not strong evidence against the presence of dust in QSOs. Also, Cardelli & Clayton (1991) and Mathis & Cardelli (1992) find that the characteristics of the 2200 Å bump and the FUV extinction rise are dramatically different on sight lines through dark clouds compared to sight lines associated with bright nebulosity, and sight lines through diffuse clouds or a mixture of dark clouds and bright nebulosity have characteristics intermediate between the pure dark cloud or pure bright nebulosity sight lines. They find that the extinction bump is quite broad on dark cloud sight lines (broader than the bump in the mean extinction curve) and quite narrow on sight lines through bright nebulosity. This suggests that the extinction bump and UV extinction are affected by the UV radiation field; perhaps UV radiation affects extinction by removing coatings from grains (Cardelli & Clayton 1991). Since the UV radiation in the vicinity of a quasar is extreme, one might expect this effect to be maximized, so it is not necessarily surprising that the redshifted 2200 Å bump is not detected in quasar spectra.

An alternative explanation of the absence of the 2200 Å bump in quasar spectra is that there are not enough small

graphite grains in the quasar environment to produce the bump. It has been suggested that the 2200 Å extinction bump is due to graphite (e.g., Stecher & Donn 1965; Mathis, Rümpl, & Nordsieck 1977), and Mathis (1994) argues that five carbon atoms for every 10^5 hydrogen atoms must be locked up in small graphite particles in order to produce the bump. If the amount of carbon in the form of small graphite particles in the immediate vicinity of the quasar is less than this amount, then the bump might not be present. In this scenario, intrinsic reddening of quasar spectra could still occur due to grains which are not composed of graphite.

If the gas-to-dust ratio in the immediate vicinity of a quasar is similar to the gas-to-dust ratio in the Milky Way, then the absence of obvious Lyman limits at the quasar emission redshifts (see Fig. 1, § 6.2, and Koratkar, Kinney, & Bohlin 1992) places tight upper limits on $E(B-V)$ (Bechtold et al. 1984). This means that if dust is present near QSOs, then (1) the gas and dust are dramatically more segregated in QSOs than they are in the Milky Way, (2) the covering factor of the dust is small and consequently the gas associated with the dust does not produce a detectable Lyman limit, or (3) the gas associated with the dust is sufficiently ionized so that the Lyman limit is not obvious. However, one must wonder if the dust is destroyed altogether if the gas is ionized to that degree. Indeed, the possibility that intrinsic reddening significantly affects broad-line region (BLR) and continuum emission is sometimes dismissed on the grounds that dust will quickly sublime in the BLR (e.g., Rudy & Puetter 1982). Laor & Draine (1993) have carried out detailed calculations of the properties of AGN dust consistent with observed spectroscopic constraints, and they suggest that large grains might exist at the outer edge of the BLR or just beyond the BLR, but this dust will not significantly redden the emission lines or continua; small grains are required for significant UV reddening. However, Laor & Draine (1993) conclude that intrinsic continuum reddening could be as high as $E(B-V) \approx 0.03$, and as we shall see, this amount of intrinsic reddening could have an important effect on the EUV spectral energy distributions of quasars.

Finally, the infrared emission of AGN between 1 and 100 μm has frequently been attributed to dust reprocessing of the UV/optical central engine emission (Rees et al. 1969; Rieke & Lebofsky 1979; Rudy 1984; Sanders et al. 1989; Laor & Draine 1993; Pier & Krolik 1993 and references therein).

In addition to intrinsic reddening due to dust in the NLR or in the immediate vicinity of the QSO central engine, intrinsic reddening could be caused by dust far-removed from the central engine in the host galaxy of the quasar. Low-density sight lines through the disk and halo of the Milky Way are moderately reddened (Cardelli & Sembach 1992), so it is not unreasonable to suggest that unobscured sight lines to QSO central engines might be reddened by the host galaxy. Small amounts of dust in elliptical galaxies are not rare (Kormendy & Djorgovski 1989 and references therein), so even an elliptical host could cause intrinsic reddening. There is evidence of intrinsic reddening in galaxies that might host quasars. For example, Calzetti, Kinney, & Storchi-Bergmann (1994) observe a correlation between the UV spectral index and the difference in the optical depths at Hα and Hβ in 39 starburst and blue compact galaxies (average redshift = 0.012). They argue that this correlation is not due to initial mass function differences, A stars from older starbursts, or selection effects, but rather is due to intrinsic continuum reddening.

The possibility that dust exists in intervening absorption line systems or the intergalactic medium is a significant complication because of the redshift smearing of the extinction. However, QSO heavy-element absorption line systems are generally assumed to originate in galaxies (which are likely to contain dust if they are spiral galaxies), and there is some evidence that dust exists in intervening absorption systems. Extinction in *individual* heavy-element systems is unlikely to be important, but the *cumulative* extinction due to all of the heavy-element absorption systems along the line of sight might be important.

4.2. *Limits on Intrinsic $E(B-V)$*

It is not clear whether intrinsic continuum reddening can be neglected in the study of AGN and quasar spectral energy distributions. For this reason, we have assembled an extinction curve which extends well into the ionizing ultraviolet (shown in Fig. 3), and we have used this extinction curve to place rough upper limits on the intrinsic continuum reddening of the quasars in Table 3. Since the 2200 Å bump generally is not detected in quasar spectra, at $\lambda \geq 912$ Å we have based our extinction curve on the Small Magellanic Cloud extinction curve (which apparently does not have a bump at 2200 Å) measured by Prévot et al. (1984). At $\lambda < 912$ Å, our extinction curve increases as ν^2 (in rough agreement with theoretical estimations based on the Kramers-Kronig relations and laboratory studies; see Draine & Lee 1984; Martin & Rouleau 1991; Laor & Draine 1993 and references therein) to a maximum at $\lambda \approx 700$ Å ($h\nu \approx 18$ eV). The EUV form of the curve is also roughly consistent with the shape of the extinction curve for small grains in the EUV inferred for the Orion Nebula by Baldwin et al. (1991). We emphasize that this is not a rigorously derived extinction curve; this is a crude estimation of the extinction which has the basic properties expected in the ion-

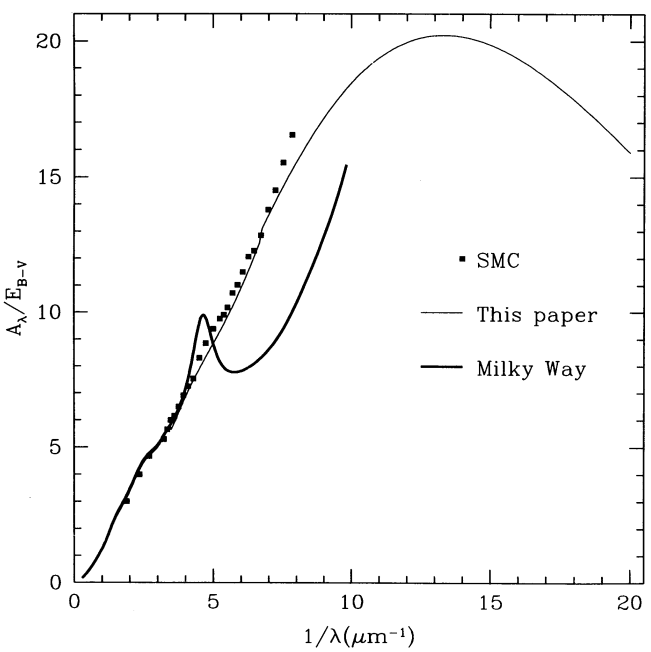

FIG. 3.—Comparison of the Small Magellanic Cloud extinction curve (*filled squares*) from Prévot et al. (1984) and the Milky Way extinction curve (*thick line*) from Cardelli, Clayton, & Mathis (1989) to the heuristic extinction curve we have assembled (*thin line*) in order to place reasonable upper limits on intrinsic quasar continuum reddening (see § 4.2 in the text).

izing ultraviolet but is not intended for accurate dereddening. Our sole purpose for this heuristic extinction curve is to derive reasonable upper limits on the amount of intrinsic continuum reddening these intermediate-redshift quasars might have undergone in order to explore the possible importance of this process.

Without the 2200 Å bump, it is difficult to determine how much intrinsic reddening a quasar continuum has undergone. We have used the following objective, but somewhat arbitrary, procedure to place reasonable upper limits on intrinsic continuum reddening. First we fit a second-degree polynomial to the optical/UV data in Table 3, using the singular value decomposition technique described by Press et al. (1992), assuming intrinsic $E(B-V) = 0$. We omitted data contaminated by emission lines or the 3000 Å bump from the data used for the fit. We also did not use the SWP data for the fit in cases where the spectral energy distribution decreased sharply in the SWP region (e.g., PG 1338+416). We then increased the assumed value of the intrinsic $E(B-V)$ and used our EUV extinction curve (see Fig. 3) to deredden the spectral energy distribution. We then refitted the polynomial. We continued to increase the intrinsic reddening correction applied to the data in Table 3 until the sign of the second derivative of the fitted polynomial changed from negative to positive. Our "upper limit" on intrinsic reddening is the intrinsic $E(B-V)$ required to just change the sign of the second derivative. Upper limits on intrinsic continuum reddening derived in this manner are listed in Table 4. Examples of the polynomial fits, before and after correcting for intrinsic reddening, are overplotted on the quasar spectral energy distributions of PG 1241+176 and PG 1630+377 in Figure 4. We have listed the spectral index which results from correcting for intrinsic continuum reddening also in Table 4.

This procedure is motivated by the fact that the big blue bump must turn over somewhere in the ionizing ultraviolet to connect with the QSO X-ray fluxes which are typically observed (e.g., Tananbaum et al. 1986; Elvis et al. 1986; Bechtold et al. 1987a; Sanders et al. 1989). For this reason, a positive UV continuum curvature in the ionizing UV is unexpected; it would lead to a complex continuum shape near the peak of the big blue bump.

Our intrinsic continuum reddening experiment yields the following results: (1) The upper limits on intrinsic $E(B-V)$ are relatively small. This is not surprising since the quasars in our sample are among the brightest quasars at intermediate redshifts. However, an apparently small color excess has a dramatic effect in the ionizing UV (see Fig. 4). Intrinsic $E(B-V) \sim 0.2$ is ruled out (for these quasars at least). It is encouraging that for six out of seven quasars, our upper limits on the intrinsic $E(B-V)$ are consistent with the upper limit set by Laor & Draine (1993) who conclude that intrinsic $E(B-V) \leq 0.03$. (2) Correcting for some intrinsic reddening causes five out of the seven quasars to have *negative* spectral indices α ($F_\nu \propto \nu^{-\alpha}$) in the optical/UV (i.e., F_ν increases with ν). This is surprising; usually quasars have positive spectral indices in this wavelength range (see Fig. 7). If most quasars undergo a small amount of intrinsic reddening that is usually not accounted for, then conclusions drawn from studies of spectral indices could be misleading. For example, Zheng & Malkan (1993) have suggested that the Baldwin effect (Baldwin 1977) is due to a dependence of the optical/UV continuum shape on quasar luminosity. This conclusion is based on their study of correlations between spectral indices and luminosity. Zheng & Malkan (1993) argue that the correlations they observe between α and L are not due to reddening, but they do acknowledge that there is some evidence that intrinsic reddening occurs in AGN and occurs even in high-luminosity quasars. Six of the seven quasars in our sample are also in the sample employed by Zheng & Malkan (1993). To illustrate how intrinsic reddening might affect spectral indices, we compare in Table 4 the spectral indices used by Zheng & Malkan (1993) to the spectral indices which result from assuming the values of intrinsic $E(B-V)$ listed in Table 4. Again we see that a small amount of intrinsic reddening can have a dramatic effect. Intrinsic reddening could also have an important effect on accretion disk models (see § 5). (3) Five out of the seven quasars have nearly the same upper limits on the intrinsic color excess, $E(B-V) \approx 0.03$. Perhaps all quasars are subjected to a small amount of "base" intrinsic reddening due to dust with a large covering factor. This base intrinsic reddening might not be obvious in the optical region of the spectral energy distribution; it may be apparent only in the ionizing UV where the extinction is maximized. If this suggestion is correct, it could be a factor in the steepening of QSO spectral energy distributions which is frequently observed in the ultraviolet. This spectral steepening is often attributed to absorption by intervening material, but on sightlines toward lower redshift quasars, sufficient intervening material may not be present. Thus lower redshift quasars detected into the ionizing UV may provide a means to test the hypothesis that quasars suffer some intrinsic continuum reddening. (4) Intrinsic continuum reddening may help resolve the apparent discrepancy between the flux emitted by the BLR and the energy input into the BLR via ionizing radiation (e.g., MacAlpine 1981; MacAlpine et al. 1985; Netzer 1985; Collin-Souffrin 1986). As first noted by MacAlpine (1981), the *observed* ionizing continuum of a typical quasar (uncorrected for intrinsic reddening) does not appear to provide enough energy to produce the observed BLR emission. MacAlpine (1981) and Netzer (1985) have suggested that BLR emission line reddening and/or continuum reddening may alleviate this energy budget problem, but Collin-Souffrin (1986) has objected to the line reddening solution on the basis of observed line ratios. Collin-Souffrin (1986) has noted that negative spectral indices in the ionizing UV may be required. Since our limits on intrinsic continuum reddening often result in negative spectral indices (see Table 4), intrinsic continuum reddening may indeed solve the problem. However, even after assuming some intrinsic reddening, many

TABLE 4

UPPER LIMITS ON INTRINSIC REDDENING

Object (1)	Intrinsic $E(B-V)$ (2)	α[a] (3)	α_{uv}[b] (4)
PG 0117+213.....	<0.028	−0.22	...
PG 1148+549.....	<0.029	−0.14	0.46
PG 1206+459.....	<0.010	0.16	1.22
PG 1241+176.....	<0.028	0.26	1.14
PG 1338+416.....	<0.045	−0.54	0.37
PG 1407+265.....	<0.028	−0.36	1.05
PG 1630+377.....	<0.026	−0.13	0.31

[a] Optical/UV spectral index ($F_\nu \propto \nu^{-\alpha}$) after correction for intrinsic reddening assuming $E(B-V)$ given in col. (2).

[b] UV spectral index employed by Zheng & Malkan (1993) assuming intrinsic reddening can be ignored.

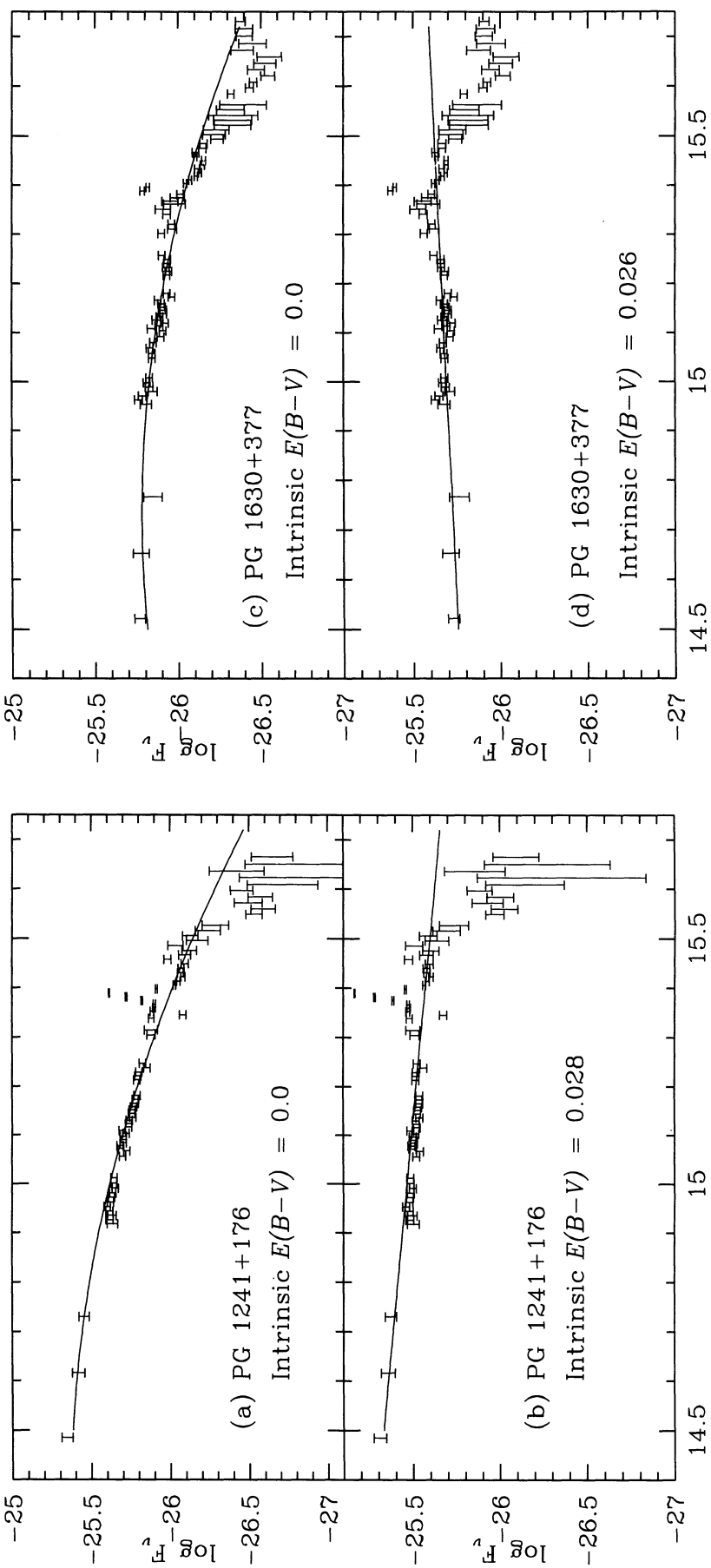

FIG. 4.—Examples of our method for placing upper limits on intrinsic reddening. We have fitted a second-order polynomial to the spectral energy distributions, corrected for Milky Way reddening, of (*a*) PG 1241+176 assuming intrinsic $E(B-V) = 0.0$, (*b*) PG 1241+176 assuming the maximum intrinsic $E(B-V)$ which can be assumed without changing the sign of the second derivative of the fitted polynomial from negative to positive (which corresponds to a change from downward curvature to upward curvature), (*c*) PG 1630+377 assuming intrinsic $E(B-V) = 0.0$, and (*d*) PG 1630+377 assuming the maximum intrinsic $E(B-V)$ which can be assumed without changing the sign of the second derivative of the fitted polynomial. Notice that assuming the upper limit on the PG 1630+377 intrinsic color excess [$E(B-V) \leq 0.026$] results in a *negative* spectral index (panel *d*).

of the spectral energy distributions turn over near the short-wavelength cutoff of the data (e.g., PG 1630+377, see Fig. 4*d*).

5. ACCRETION DISK MODELS

In this section we explore some implications of the spectral energy distributions tabulated in Table 3 on accretion disk models of the quasar central engine. To illustrate the degree of uncertainty in accretion disk parameters introduced by uncertainty in the cosmological parameters, we carry out all calculations in this section for two cases, the first case assuming $H_0 = 100$ km s^{-1} Mpc^{-1} and $q_0 = 0.5$ and the second case assuming $H_0 = 50$ km s^{-1} Mpc^{-1} and $q_0 = 0.1$.

We begin with the simple geometrically thin optically thick accretion disk model described by Bechtold et al. (1987a). As shown by Bechtold et al. (1987a; these equations were originally derived by B. Czerny), in the classical physically thin accretion disk in which the local disk spectrum is approximated by a blackbody, the black hole mass, M_{BH}, and the accretion rate, $\dot{M}$, can be related to observables by the following equations:

$$\log\left(\frac{M_{BH}}{M_\odot}\right) = -\log\left(\frac{\dot{M}}{M_\odot\ \mathrm{yr}^{-1}}\right) + \frac{3}{2}(\log L_{\nu_0} - 19.222) - \frac{1}{2}\log \nu_0\ , \quad (2)$$

and

$$\log\left(\frac{M_{BH}}{M_\odot}\right) = 39.189 + \frac{1}{2}\log\left(\frac{\dot{M}}{M_\odot\ \mathrm{yr}^{-1}}\right) - 2\log \nu_{max}\ , \quad (3)$$

where L_{ν_0} is the luminosity at some frequency ν_0 in the power-law region of the big blue bump (we use L_{ν_0} at $\log \nu_0 = 15.315$) and ν_{max} is the frequency at which νL_ν is a maximum. These equations apply to a nonrotating black hole and assume $\cos i \approx 0.5$ (i is the inclination of the disk). The black hole masses and accretion rates derived from these equations for six of the quasars in Table 3 (we do not include PG 1407+265 in this analysis because of the uncertainty of its redshift) and the nine quasars in the sample of Bechtold et al. (1984) are plotted in Figure 5, assuming intrinsic $E(B-V) = 0$ (we include intrinsic reddening below). The filled squares in this figure were calculated assuming $H_0 = 100$ km s^{-1} Mpc^{-1} and $q_0 = 0.5$ and the open squares were calculated assuming $H_0 = 50$ km s^{-1} Mpc^{-1} and $q_0 = 0.1$. To illustrate the impact of choosing different H_0 and q_0 values, the PG 1241+176 M_{BH} and $\dot{M}$ calculated with the two sets of cosmological parameters are connected with a dashed line in Figure 5. Changing the cosmological parameters changes the black hole mass by roughly a factor of 2 and changes the accretion rate by almost an order of magnitude.

Unfortunately, the peak of the big blue bump is usually difficult to definitively identify, and for the most part only lower limits can be placed on ν_{max}. Often νL_ν continues to increase all of the way down to the short-wavelength cutoff of the *IUE* spectra. Also, the apparent peak of the big blue bump may not be the true turnover. The apparent turnover may be due to intrinsic reddening or intervening absorption, for example. For this reason, the M_{BH} and $\dot{M}$ derived from equations (2) and (3) are limits; increasing the lower limit on ν_{max} will increase M_{BH} and $\dot{M}$ in the direction indicated by an arrow on each point in Figure 5.

The geometrically thin accretion disk model for QSOs has often been criticized on the grounds that it requires luminosities in excess of the Eddington luminosity, which will puff up the disk so that the model is not self-consistent. Figure 5 corroborates this criticism. For a given black hole mass, the accretion rate at which $L = L_{Edd}$, the "Eddington accretion rate," is given by

$$\dot{M}_{Edd} = \frac{4\pi G m_p}{c\eta\sigma_{es}} M_{BH}\ , \quad (4)$$

where σ_{es} is the electron scattering cross section, m_p is the proton mass, η is the efficiency of energy release, and the other symbols have their usual meanings. For a nonrotating (Schwarzschild) black hole, $\eta = 5.7\%$. We have indicated the critical accretion rate given by equation (4) by a heavy line in Figure 5. Sources with M_{BH} and $\dot{M}$ below and to the right of this heavy line will have $L > L_{Edd}$. From Figure 5 we see that if $H_0 = 100$ km s^{-1}Mpc^{-1} and $q_0 = 0.5$, then eight out of the 15 quasars exceed the Eddington luminosity, and if $H_0 = 50$ km s^{-1} Mpc^{-1} and $q_0 = 0.1$, then 14 out of the 15 quasars exceed the Eddington luminosity or accrete with $L \approx L_{Edd}$.

A small amount of intrinsic reddening exacerbates this problem with the thin accretion disk model. Correcting for intrinsic reddening increases L_{ν_0} and ν_{max} in equations (2) and (3), which increases M_{BH} and $\dot{M}$ and thereby pushes the quasar toward the $L > L_{Edd}$ region in Figure 5. Increasing ν_{max} also pushes the QSO toward the super-Eddington regime. Table 5

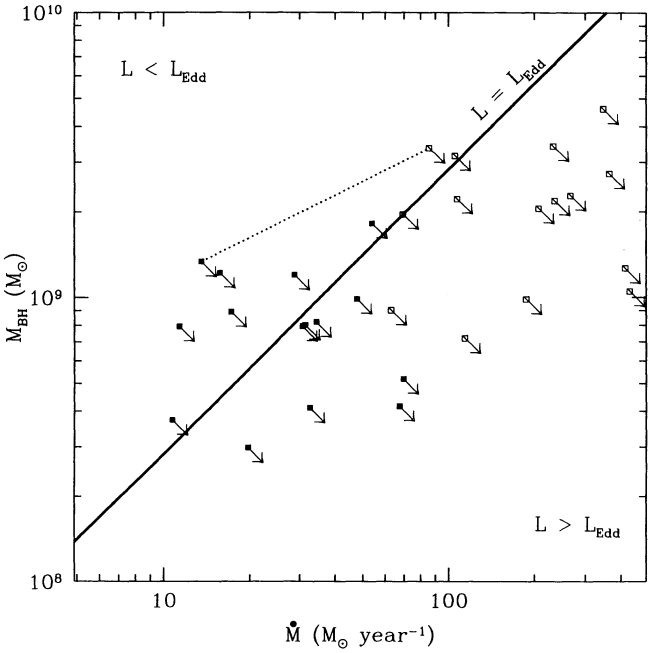

FIG. 5.—Black hole masses (M_{BH}) and accretion rates ($\dot{M}$) derived from a geometrically thin optically thick accretion disk model. The accretion disk parameters are derived from the data in Table 3 and the data given by Bechtold et al. (1984). This model requires an estimation of ν_{max}, the frequency at which νL_ν is maximized. Since only lower limits can be placed on ν_{max}, the points plotted here are also limits. Increasing ν_{max} increases M_{BH} and $\dot{M}$ in the direction indicated by an arrow on each point. The heavy line shows the accretion rate at which $L = L_{Edd}$ for a given black hole mass. Points below and to the right of this line require super-Eddington accretion rates. The filled squares assume $H_0 = 100$ km s^{-1} Mpc^{-1} and $q_0 = 0.5$, and the open squares assume $H_0 = 50$ km s^{-1} Mpc^{-1} and $q_0 = 0.1$. To emphasize the uncertainty introduced by the uncertain values of the cosmological parameters, we have connected the accretion disk parameters calculated for PG 1241+176 for the two sets of (H_0, q_0) with a dashed line.

TABLE 5

ACCRETION RATES AND BLACK HOLE MASSES

Object	H_0 (km s^{-1} Mpc^{-1})	q_0	Intrinsic $E(B-V)$	M_{BH} (10^8 $M_\odot$)	$\dot{M}$ ($M_\odot$ yr^{-1})	$\dot{M}_{Edd}$ ($M_\odot$ yr^{-1})
PG 0117+213.....	100	0.5	0.0	7.9	31	28
	100	0.5	0.028	12	73	43
	50	0.1	0.0	20	206	71
	50	0.1	0.028	32	493	114
PG 1148+549.....	100	0.5	0.0	4.1	33	15
	100	0.5	0.029	6.4	79	23
	50	0.1	0.0	9.8	187	35
	50	0.1	0.029	15	456	53
PG 1206+459.....	100	0.5	0.0	7.9	11	28
	100	0.5	0.010	6.9	20	24
	50	0.1	0.0	20	69	71
	50	0.1	0.010	17	125	60
PG 1241+176.....	100	0.5	0.0	13	14	46
	100	0.5	0.028	21	32	75
	50	0.1	0.0	34	86	121
	50	0.1	0.028	52	205	185
PG 1338+416.....	100	0.5	0.0	8.9	17	32
	100	0.5	0.045	14	90	50
	50	0.1	0.0	22	107	78
	50	0.1	0.045	34	557	121
PG 1630+377.....	100	0.5	0.0	12	16	43
	100	0.5	0.026	12	53	43
	50	0.1	0.0	31	105	110
	50	0.1	0.026	31	354	110

NOTES.—M_{BH} and $\dot{M}$ were derived from the geometrically thin accretion disk model described by Bechtold et al. 1987a. $\dot{M}_{Edd}$ is the Eddington accretion rate at which $L = L_{Edd}$ for the given M_{BH}.

lists the black hole masses and accretion rates derived from equations (2) and (3) for the six quasars in Table 3 (again excluding PG 1407+265) assuming intrinsic $E(B-V) = 0.0$ and assuming the intrinsic $E(B-V)$ equals the upper limit derived in § 4.2. We see that for the $H_0 = 100$ and $q_0 = 0.5$ case including intrinsic reddening, four out of the six quasars exceed L_{Edd}, and for the $H_0 = 50$ and $q_0 = 0.1$ case with intrinsic reddening, all six quasars exceed L_{Edd}. The reasonable possibility that luminous quasars undergo a small amount of intrinsic reddening poses a severe problem for this model. We note that PG 1206+459, PG 1241+176, and PG 1630+377 do not require super-Eddington accretion rates unless the intrinsic reddening in Table 4 is assumed.

Czerny & Elvis (1987) have pointed out that electron scattering opacity effects can relieve the super-Eddington accretion rate problem in the thin disk model, so we now proceed to compare our data to more sophisticated accretion disk models. Electron scattering extends the disk spectrum to shorter wavelengths compared to a blackbody at the same effective temperature (see Fig. 1 in Czerny & Elvis 1987 or Fig. 1 in Wandel & Petrosian 1988). Wandel & Petrosian (1988) have carried out accretion disk modeling similar to the calculations of Czerny & Elvis (1987). For accretion disks viewed face-on, Wandel & Petrosian (1988) have calculated the luminosity and spectral index at 1450 Å for a grid of black hole masses and accretion rates. This grid is shown in Figures 6–8 where we plot α(1450 Å) versus L_ν(1450 Å). The solid lines in Figures 6–8 are curves of constant black hole mass, and the dashed lines are curves of constant dimensionless accretion rate $\dot{m}$ defined as

$$\dot{m} = \dot{M}c^2/L_{Edd} , \quad (5)$$

so that

$$L = \eta \dot{m} L_{Edd} . \quad (6)$$

The advantage of this method of presenting the results of accretion disk modeling is that the accretion disk parameters can be visually compared to observable spectral properties, and trends should be apparent in the plot.

The data obtained by Seyfert galaxy reverberation monitoring campaigns (see Peterson 1993 for a recent review) can be used as a consistency check of the accretion disk model calculated by Wandel & Petrosian (1988). Seyfert galaxies show rapid continuum variability. If this continuum variability is due to variability of the accretion rate, then the α(1450 Å) versus L_ν(1450 Å) data from Seyfert reverberation monitoring programs should move back and forth along a line of constant black hole mass when overplotted on Wandel & Petrosian's grid of accretion disk models. In Figure 6*a* were have overplotted the data from reverberation monitoring of NGC 5548 (Clavel et al. 1991)[4] on the $M_{BH} - \dot{m}$ accretion disk grid computed by Wandel & Petrosian (1988) assuming the disk viscosity parameter = 0.1 and including the effects of electron scattering and Comptonization. The open stars in this and the following figure assume $H_0 = 100$ and $q_0 = 0.5$, and the filled squares assume $H_0 = 50$ and $q_0 = 0.1$. In Figure 6*b* we have overplotted the data from reverberation monitoring of NGC 3783 (Reichert et al. 1994) on the same grid. From these figures we see that to within the scatter in the measurements, the Seyfert data appear to lie roughly on curves of constant black hole mass, and this gives us confidence in the accretion disk models of Wandel & Petrosian (1988).

We overplot α(1450 Å) versus L_ν(1450 Å) derived from the data in Table 3 on the Wandel & Petrosian (1988) accretion disk grid in Figures 7 and 8 (Fig. 7 assumes $H_0 = 100$ and $q_0 = 0.5$ while Fig. 8 assumes $H_0 = 50$ and $q_0 = 0.1$). Figures

[4] Clavel et al. (1991) report fluxes at 1337 Å, and we have estimated the flux at 1450 Å by using their measured spectral indices to extrapolate.

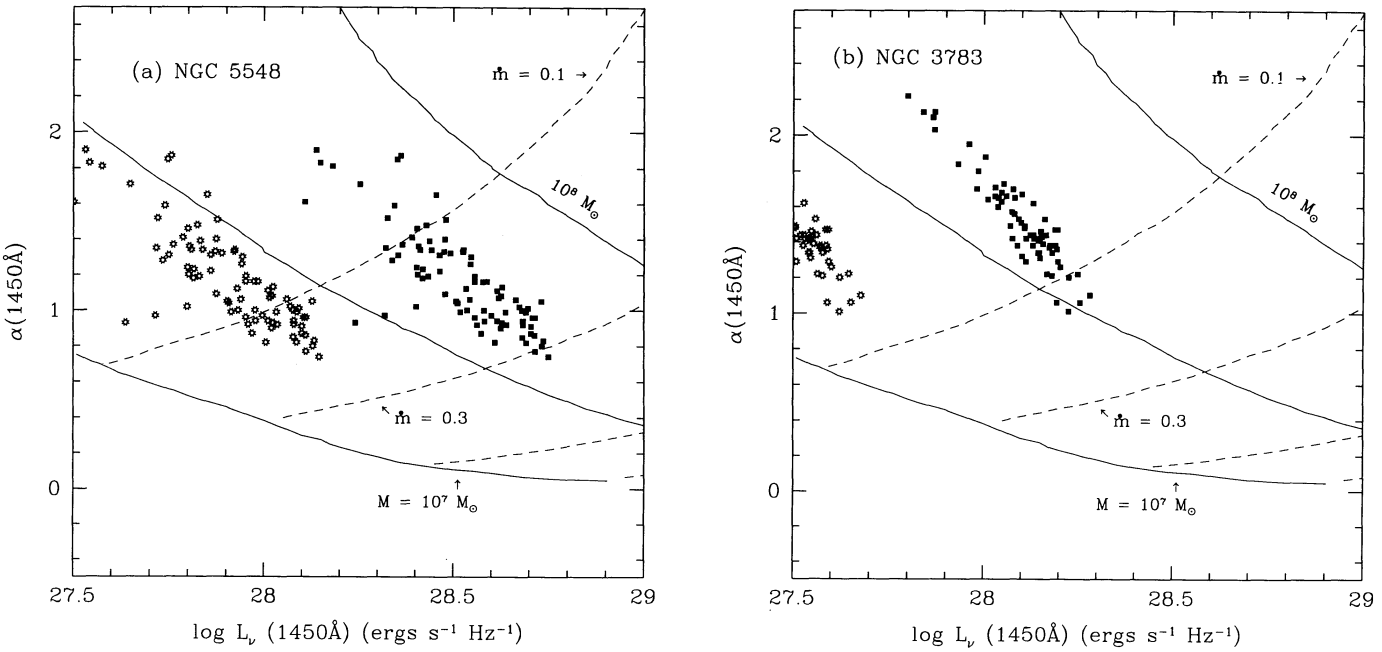

FIG. 6.—The variable spectral index (α) and luminosity at 1450 Å observed by (*a*) the NGC 5548 reverberation monitoring campaign (Clavel et al. 1991), and (*b*) the NGC 3783 reverberation monitoring campaign (Reichert et al. 1994) overplotted on the luminosity and spectral index at 1450 Å calculated by Wandel & Petrosian (1988) for accretion disk models assuming a range of black hole masses and accretion rates. The solid lines are curves of constant black hole mass and the dashed lines are curves of constant dimensionless accretion rate $\dot{m}$ ($\dot{m} = \dot{M}c^2/L_{\rm Edd}$). This model assumes that the accretion disk viscosity parameter = 0.1 and includes electron scattering opacity effects and Comptonization. The observational data appear to lie roughly on curves of constant black hole mass. The open stars assume $H_0 = 100$ km s^{-1} Mpc^{-1} and $q_0 = 0.5$, and the filled squares assume $H_0 = 50$ km s^{-1} Mpc^{-1} and $q_0 = 0.1$.

7*a* and 8*a* show the Wandel & Petrosian (1988) accretion disk grid which results from assuming that the accretion disk viscosity parameter is less than 0.01. In this model electron scattering is not important, and the disk is modeled as a multitemperature blackbody. Therefore the model in Figures 7*a* and 8*a* is similar to the Bechtold et al. (1987a) model. Figures 7*b* and 8*b* show the Wandel & Petrosian (1988) grid which results from assuming that the accretion disk viscosity parameter is 0.1. The model includes the effects of electron scattering and Comptonization. Unfortunately, the grid published by Wandel & Petrosian (1988) only extends up to $\dot{m} = 10$ for this model. The α(1450 Å) and L_ν(1450 Å) derived from the data in Table 3 are indicated by large filled squares in Figures 7 and 8.

Since fluxes and spectral indices at 1450 Å are often published, we have also plotted in Figures 7 and 8 α(1450 Å) versus L_ν(1450 Å) from the literature on quasars and Seyfert galaxies. In Figures 7 and 8, filled triangles are Seyfert galaxies from Wu, Boggess, & Gull (1983, using the spectral indices from Cheng, Gaskell, & Koratkar 1991), Clavel & Joly (1984), and Edelson, Krolik, & Pike (1990); the open squares are quasars with $z_{\rm em} < 1.0$ from Green et al. (1980), Kinney et al. (1985), Cheng & Fang (1987), and O'Brien, Gondhalekar, & Wilson (1988b); the filled squares are quasars with $1.0 \leq z_{\rm em} < 2.0$ from Bechtold et al. (1984), O'Brien et al. (1988b), and this paper; the open stars are quasars with $z_{\rm em} \geq 2.0$ from Osmer & Smith (1976, 1977 with spectral indices estimated by Cheng et al. 1991), Bechtold et al. (1984), Sargent, Steidel, & Boksenberg (1989), and Pei, Fall, & Bechtold (1991).

For a Schwarzschild black hole, $\dot{m} > 17.5$ is a super-Eddington accretion rate (see eq. [6]). Therefore in Figure 7*a*, 13 out of the 177 quasars plotted require super-Eddington accretion rates, while in Figure 8*a*, 28 out of the 177 quasars

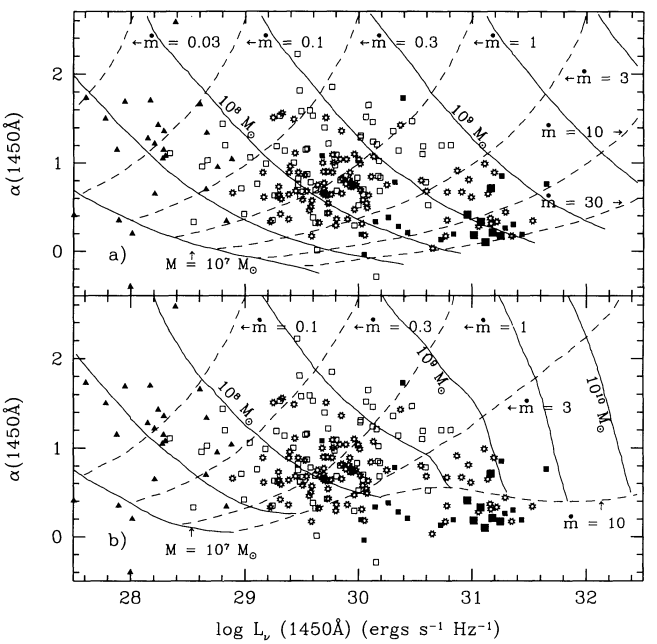

FIG. 7.—Comparison of the α(1450 Å) vs. L_ν(1450 Å) derived from the data in Table 3 (*large symbols*) and the literature (*small symbols*) to the accretion disk parameter grid calculated by Wandel & Petrosian (1988) for models that (*a*) assume the accretion disk viscosity parameter is less than 0.01 and treat the local disk spectrum as a blackbody (i.e., electron and Compton scattering effects are not included), and (*b*) assume the accretion disk viscosity parameter = 0.1 and include electron scattering and Comptonization. The filled triangles are Seyfert galaxies, open squares are quasars with $z_{\rm em} < 1.0$, filled squares are quasars with $1.0 \leq z_{\rm em} < 2.0$, and the open stars are quasars with $z_{\rm em} \geq 2.0$. Literature sources are listed in the text. In this figure, luminosities were calculated assuming $H_0 = 100$ and $q_0 = 0.5$.

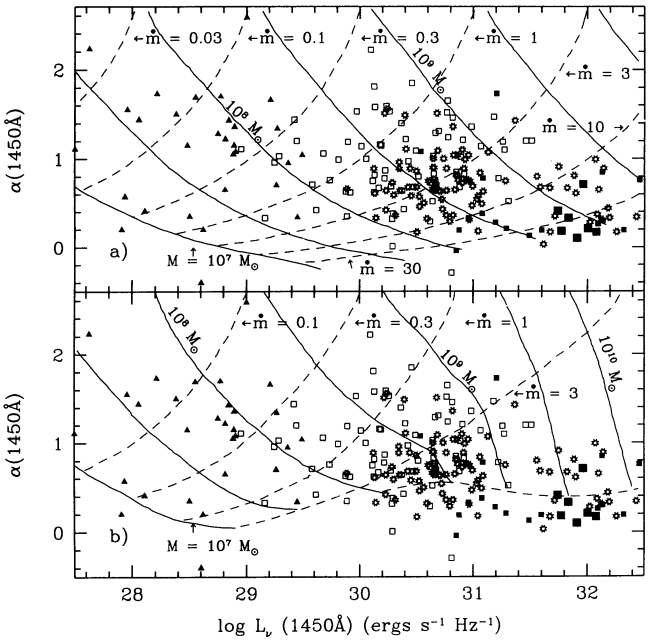

FIG. 8.—Same as Fig. 7, except luminosities were calculated assuming $H_0 = 50$ and $q_0 = 0.1$.

require super-Eddington accretion rates. This reveals a selection effect. Ostensibly, the disk model calculated by Wandel & Petrosian (1988) has statistically less trouble with super-Eddington accretion rates than the model employed by Bechtold et al. (1987a). This is not true. Eight of the 13 quasars in Figure 7*a* and 14 of the 28 quasars in Figure 8*a* that require super-Eddington accretion rates are from this paper or Bechtold et al. (1984). We have selected the brightest intermediate-redshift PG quasars because they can be detected with the *IUE*, and thus we have also selected the QSOs most likely to require super-Eddington accretion rates. The previous discussion of accretion rates derived from equations (2) and (3) should not be interpreted as an indication that the majority of quasars require super-Eddington accretion rates inconsistent with the model assumptions. Figures 7*a* and 8*a* indicate that ~7%–16% of quasars require $L > L_{\rm Edd}$ in the geometrically thin accretion disk model. However, we have again neglected the possibility that many quasars suffer some intrinsic continuum reddening in Figures 7 and 8. It is well known that lower luminosity quasars have higher X-ray to optical luminosity ratios (e.g., Avni & Tananbaum 1986; Schmidt & Green 1986 and references therein), and this anticorrelation of $L_X/L_{\rm Opt}$ with L_V might be indirectly related to intrinsic continuum reddening. The Baldwin effect (e.g., Baldwin 1977; Baldwin, Wampler, & Gaskell 1989), as observed at various levels for all of the major UV emission lines, can be interpreted as evidence that the covering factors of the BLR and NLR increase as the optical luminosity decreases (Mushotzky & Ferland 1984), possibly due to radiation pressure, mass ejection, or both. If there is dust associated with the gas in either or both of these regions, then intrinsic reddening might be greater in lower luminosity objects. Alternatively, the Baldwin effect might not be due to changing covering factors of the BLR and NLR, but instead might be due to intrinsic reddening alone (Shuder & MacAlpine 1979). In either case, intrinsic reddening could require a significant fraction of the quasars in Figures 7 and 8 to have super-Eddington accretion rates after all. It is difficult to estimate how many quasars exceed $L_{\rm Edd}$ when electron scattering opacity effects are included in the model (Figs. 7*b* and 8*b*) because Wandel & Petrosian (1988) published only curves of constant accretion rate up to $\dot{m} = 10$. Comparison of the grids in Figures 7*a* and 7*b* clearly shows that higher luminosities can be obtained without exceeding $\dot{M}_{\rm Edd}$ if electron scattering is included (consistent with the findings of Czerny & Elvis 1987).

Some clear, if unsurprising, trends are apparent in Figures 7 and 8. Only Seyfert galaxies and a few low-redshift ($z_{\rm em} < 1.0$) QSOs have $\log L_\nu < 29$, only intermediate and high-redshift quasars are observed at the highest luminosities, and the spectral energy distributions appear to grow flatter with increasing luminosity and/or redshift (α[1450 Å] decreases with luminosity and/or redshift). We refer the reader to Caditz (1993) for a discussion of the luminosity evolution of low and intermediate-redshift quasars in the context of accretion disk models.

6. INTERGALACTIC ABSORPTION

6.1. *A Composite Spectrum for the* He I *Gunn-Peterson Test*

To date, three quasars have been used to place upper limits on the smoothly distributed intergalactic neutral helium density using the Gunn & Peterson (1965) test. Tripp, Green, and Bechtold (1990) have used multiple *IUE* observations of PG 1115+080 ($z_{\rm em} = 1.722$) to place an upper limit on the optical depth of the Gunn-Peterson trough, and they find that $\tau_{\rm GP,He\,I} < 0.21$ at the 3 σ level. Beaver et al. (1991) have used four observations of UM 675 ($z_{\rm em} = 2.148$) made with the *HST* FOS to carry out this test, and they find that $\tau_{\rm GP,He\,I} < 0.27$ at the 3 σ level. Recently, the $z_{\rm em} = 3.544$ QSO OQ172 has been detected with the FOS down to 323 Å in the rest frame (Beaver et al. 1992; Lyons et al. 1992), but at the time of this writing a limit on $\tau_{\rm GP,He\,I}$ derived from the OQ172 spectrum had not been published. Using equation (1) from Tripp et al. (1990), these optical depth limits can be converted into upper limits on the number density of smoothly distributed intergalactic He I, and then model-dependent lower limits can be placed on the temperature of the intergalactic medium (e.g., Ikeuchi & Ostriker 1986; Tripp et al. 1990) and/or the metagalactic ionizing background radiation (e.g., Miralda-Escudé & Ostriker 1990, 1992; Bechtold et al. 1987b; Madau 1992; Terasawa 1992). Reimers et al. (1989) have detected HS 1700+6416 ($z_{\rm em} = 2.72$) down to 330 Å in the rest frame, but they did not place a limit on $\tau_{\rm GP,He\,I}$ because the continuum is not sufficiently well detected with the *IUE* between $\lambda_{\rm rest} \sim 450$ Å and 850 Å. However, Reimers et al. (1992) have obtained a spectacular spectrum of HS 1700+6416 with the FOS. In this recently obtained FOS spectrum the continuum is well detected in the vicinity of 584 Å in the rest frame, and the He I Gunn-Peterson trough is not observed. Reimers et al. (1992) conclude that $n_{\rm He\,I} \leq 7 \times 10^{-12}$ cm^{-3} at $z = 2.72$ (assuming $q_0 = 0$ and $H_0 = 50$ km s^{-1} Mpc^{-1}).

Additional quasars suitable for the He I Gunn-Peterson test (i.e., quasars whose continuum emission is detected below 584 Å in the rest frame) have been observed. Additional QSOs detected by *IUE* which are suitable for the He I Gunn-Peterson test are PHL 1377, PG 0946+301, Ton 34, PG 1338+416, PG 1522+101, and PG 1630+377. PG 0946+301 ($z_{\rm em} = 1.216$) is a broad absorption line QSO and consequently the continuum level is difficult to determine in the vicinity of the He I Gunn-Peterson trough. The *IUE* observations of these

quasars (excluding the BAL QSO) are summarized in Table 1 along with their emission redshifts, visual magnitudes, and sight line H I column densities. The spectra of these quasars, reduced as described in § 2, are shown in Figure 1. Ironically, of this list of QSOs detected with *IUE* below $\lambda_{rest} = 584$ Å, PG 1115+080 appears to suffer the worst Hackney et al. (1982) continuum distortion.

We have combined, weighted by the S/N, the spectra of these QSOs detected with *IUE* at and below $\lambda_{rest} = 584$ Å in order to build a composite spectrum which we have used to place an improved limit on $\tau_{GP,He\,I}$. We have included the co-added spectrum of PG 1115+080 from Tripp et al. (1990) in this composite spectrum, but we have not included PG 1338+416 since rest frame 584 Å is just barely redshifted above geocoronal Lyα emission in that spectrum. For one reason or another, the QSO continua we have combined to form this composite spectrum have different shapes, so we normalized the individual spectra using the best-fit fourth order Chebyshev polynomial (fitted to the entire SWP spectrum) before co-adding them in the rest frame. The resultant normalized spectrum is plotted versus rest frame wavelength in Figure 9. For purposes of comparison, we also show the normalized spectrum of PG 1115+080 from Tripp et al. (1990) in Figure 9. By co-adding the different quasar spectra in the rest frame, the fixed pattern noise, continuum distortion, and camera artifacts are smeared out (since the quasars have different redshifts), and we can see from Figure 9 that the S/N is clearly improved. The disadvantage of using this composite spectrum to place a tighter limit on $\tau_{GP,He\,I}$ is that the limit applies to a mean redshift of $\langle z \rangle = 1.58$. Since the depth of the Gunn-Peterson trough is expected to increase with increasing redshift (especially if the intergalactic medium is photoionized by quasars; see Figure 1 in Jenkins & Ostriker 1991), it is of greatest interest to place limits on τ_{GP} at the highest possible redshift. At any rate, using the composite spectrum in Figure 9 and the same method employed by Tripp et al. (1990), we find that $\tau_{GP,He\,I} \leq 0.09$ at the 3 σ level.

According to the calculations of Shapiro & Giroux (1987), the number of quasars observed at high redshift is insufficient to ionize the intergalactic medium to the degree required by the H I Gunn-Peterson test. In response to this conclusion, Sciama (1988) and Melott, McKay, & Ralston (1988) have suggested that photons emitted by decaying dark matter (heavy neutrinos or photinos) might be an important source of photoionization of the IGM. If the decaying dark matter is neutrino-like, then Sciama (1990) expects the energy of the emitted photons to be 13.8 ± 0.2 eV. Sciama (1988) also points out that decaying dark matter could provide the excess photoionizing flux (in addition to the contribution from observed quasars) apparently required to satisfy the "proximity effect" observed in the Lyα forest (Bajtlik, Duncan, & Ostriker 1988; Miralda-Escudé & Ostriker 1990; Madau 1992; however, see Miralda-Escudé & Ostriker 1992; Terasawa 1992; Espey 1993; Bechtold 1994). This dark matter hypothesis appears to be inconsistent with the upper limit on $\tau_{GP,He\,I}$ presented in this paper and derived from recent *HST* observations. Decaying dark matter emitting 13.8 eV photons would not be able to ionize intergalactic neutral helium (the ionization potential of He I is 24.6 eV), so the He I Gunn-Peterson trough should be easily detected (assuming the IGM has a big bang primordial helium abundance). However, quasars alone may be able to ionize all of the intergalactic He I even if they can not ionize all of the intergalactic H I, and there may be additional important sources of ionization such as shock heating (e.g, Ikeuchi & Ostriker 1986) or cosmic rays (Ginzberg & Ozernoy 1966; Nath & Biermann 1993). Miralda-Escudé & Ostriker (1990, 1992) have examined models of the ionizing background radiation including various combinations of flux from observed quasars, hidden quasars, young stars in primordial galaxies, and decaying heavy neutrinos. They conclude that ionizing radiation from quasars and decaying neutrinos can ionize the smoothly distributed IGM, but a large fraction of helium in the Lyα forest will remain unionized and He I absorption lines should be easily detected in the Lyα clouds. *IUE* QSO data do not have high enough resolution and S/N for detection of discrete He I absorption lines, but our technique of combining several quasar spectra to form a composite spectrum could lead to a detectable flux decrement in the composite due to the build-up of undetected lines in the individual spectra. At $z < 2$ this is not likely because there are not sufficiently many Lyα clouds in this redshift range, but this may be a useful technique for searching for helium in the Lyα forest in higher redshift *HST* spectra.

Cen, Ostriker, and collaborators (Cen et al. 1991; Cen & Ostriker 1992a, b, 1993; Cen, Ostriker, & Peebles 1993a; Cen, Gnedin, & Ostriker 1993b) have demonstrated the usefulness of the He I Gunn-Peterson test for constraining hot and cold dark matter cosmologies. In several of their three-dimensional hydrodynamic simulations, they find that $\tau_{GP,He\,I}$ predicted by the model is considerably larger than the upper limit set by Tripp et al. (1990) while in other models the observed limit is satisfied.

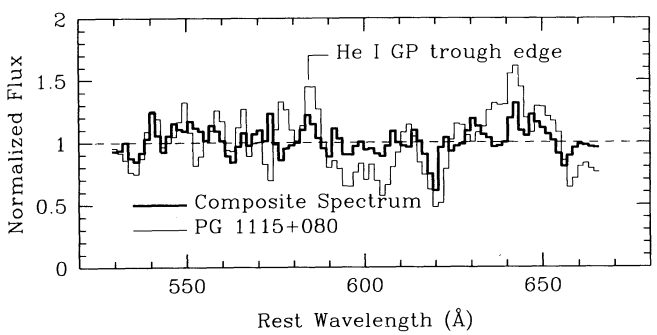

FIG. 9.—A composite spectrum (*heavy line*) formed from *IUE* observations of PHL 1377, Ton 34, PG 1115+080, PG 1522+101, and PG 1630+377. We have used this composite spectrum to carry out an improved He I Gunn-Peterson test. For purposes of comparison, we show the normalized spectrum of PG 1115+080 used previously by Tripp, Green, & Bechtold (1990) for the He I Gunn-Peterson test.

6.2. *Intermediate-Redshift Lyman Limits*

The spectra of five of the quasars shown in Figure 1 contain continuum discontinuities which are probably Lyman limit systems (i.e., absorption systems with a significant optical depth to Lyman continuum radiation). These Lyman limit systems are listed in Table 6 along with associated heavy-element absorption lines from observations in the literature, our estimations of their redshifts, and limits on their optical depths and neutral hydrogen column densities. We have determined the optical depth of a given Lyman limit system from

$$\tau_{LL} = -\ln\left[\frac{F(\lambda_-)}{F(\lambda_+)}\right], \quad (7)$$

TABLE 6

INTERMEDIATE REDSHIFT LYMAN LIMIT SYSTEMS

QSO	z_{LL}[a]	τ_{LL}	$N_{H\,I}$ (cm^{-2})	Associated Heavy Elements
PG 0117+213	1.4–1.49	>0.7	$>1.4 \times 10^{17}$	...
Ton 34	1.6	0.5 ± 0.2	$(8.5 \pm 3.4) \times 10^{16}$	C II[b], C IV[b,c], S IV[b]
PG 1241+176	0.5–0.6	>1.0	$>2.1 \times 10^{17}$	...
PG 1248+401	0.8	>1.1	$>2.3 \times 10^{17}$	Mg II[d]
PG 1715+535	1.6	>0.6	$>1.1 \times 10^{17}$	Si II[b], C IV[b]

[a] Determined from associated heavy element absorption lines when possible; otherwise computed from *IUE* LL edge.

[b] Sargent, Boksenberg, & Steidel 1988.

[c] Young, Sargent, & Boksenberg 1982.

[d] Bechtold et al. 1984.

where $F(\lambda_-)$ is the flux at wavelengths below and $F(\lambda_+)$ is the flux at wavelengths above the Lyman limit. Only one of the quasars (Ton 34) shows a detectable continuum below the Lyman limit (however, see § 3.1); for the other quasars we have used the flux uncertainties estimated in § 2 to place 3 σ limits on $F(\lambda_-)$. Since the cross section for photoionization of H I is

$$\sigma = 6.25 \times 10^{-18}\left(\frac{\langle\lambda\rangle}{912\ \text{Å}}\right)^3\ \text{cm}^2\ , \qquad (8)$$

where $\langle\lambda\rangle$ is the average wavelength of the region used to determine $F(\lambda_-)$, the H I column density associated with a Lyman limit is

$$N_{H\,I} = 1.6 \times 10^{17}\left(\frac{912\ \text{Å}}{\langle\lambda\rangle}\right)^3 \tau_{LL}\ \text{atoms cm}^{-2}\ . \qquad (9)$$

We noted in § 3.1 that the spectra of PG 1206+459, PG 1338+416, and PG 1630+377 contain broad dips which could be Lyman limit systems. At first glance, these broad dips look like the broad absorption trough that Møller & Jakobsen (1990) have suggested might be produced by the cumulative Lyman continuum absorption in the Lyα forest, the so-called "Lyman valley." However, we have used Møller & Jakobsen's equation (9) to estimate the depth of the Lyman valley, and we find that it is not likely to be important at these redshifts and cannot produce deep enough absorption troughs to explain the features observed in the SWP spectra of these quasars.

A possible problem with the accretion disk model of the quasar central engine is that a partial Lyman limit at the emission redshift of the quasar is predicted by many renditions of this model. Koratkar et al. (1992) have carried out a search for partial Lyman limits at the emission redshift in the spectra of 49 quasars observed with *IUE*. Only five of these quasars, including PG 0117+213 and PG 1338+416, show possible Lyman limits near z_{em} that do not have associated absorption systems. Since the PG 0117+213 Lyman limit is not a partial Lyman limit (i.e., no continuum flux is detected blueward of the Lyman limit), Koratkar et al. (1992) conclude that this Lyman limit does not originate in an accretion disk. The PG 1338+416 *IUE* spectrum does contain a broad absorption trough near the expected position of a Lyman limit at z_{em} (see Fig. 1), but this quasar has been observed with the *HST* FOS as part of the Quasar Absorption Line Key Project, and the Key Project automated Lyman limit identification procedure (see Schneider et al. 1993) does not identify this broad absorption feature as a Lyman limit system. The Key Project Lyman limit search has identified a Lyman limit in the spectrum of PG 1206+459 at $z_{LL} = 1.158$ (Bahcall et al. 1993).

7. SUMMARY

In summary, the principal results of this paper are the following:

1. We have compiled the near-IR–UV spectral energy distributions of seven of the brightest quasars at intermediate redshifts ($0.94 \leq z_{em} \leq 1.5$) in the Palomar-Green survey using the spectrophotometry of Neugebauer et al. (1987) and *International Ultraviolet Explorer* spectra. We have corrected the spectral energy distributions for Milky Way reddening by using the observed N(H I) on each sight line to determine $E(B-V)$.

2. After reviewing some of the literature on dust in AGN, we have set upper limits on the intrinsic continuum reddening of these quasars. For this purpose, we have put together an extinction curve which extends to $\lambda \ll 912$ Å. At $\lambda > 912$ Å, this extinction curve is based on the extinction observed in the Small Magellanic Cloud because the redshifted 2200 Å bump is not detected in quasar spectra. At $\lambda < 912$ Å, the extinction curve roughly follows theoretical expectations. Using this extinction curve, we have derived reasonable upper limits on the intrinsic $E(B-V)$ for each quasar based on the maximum amount of dereddening which can be applied without giving the big blue bump a complex shape. Specifically, we have determined the maximum intrinsic $E(B-V)$ which can be assumed without changing the curvature of a second-degree polynomial, fitted to the spectral energy distribution after dereddening, from downward to upward. For six out of the seven quasars, we find that intrinsic $E(B-V) < 0.03$, and the seventh QSO requires $E(B-V) < 0.045$. These color excesses are relatively small by Galactic standards, but this amount of intrinsic reddening has a dramatic effect on the EUV spectral energy distributions. We have discussed some implications of our intrinsic reddening upper limits.

3. We have used geometrically thin accretion disk models to derive the black hole masses and accretion rates required to produce the observed spectral energy distributions. We find that a large fraction of the brightest PG quasars at intermediate redshifts require super-Eddington accretion rates (which is not consistent with the thin disk assumption) even if intrinsic reddening is negligible. Since we have selected the brightest quasars, we may have selected the QSOs most likely to exceed the Eddington limit. However, we may have also selected the quasars with the least intrinsic continuum reddening. If intrinsic reddening is important, then a large fraction of quasars may require $L > L_{Edd}$ in thin accretion disk models. We also plot the recent data resulting from reverberation monitoring of the Seyfert galaxies NGC 5548 and NGC 3783 on the grid of

accretion disk models produced by Wandel & Petrosian (1988). We find that to within the scatter in the measurements, the Seyfert galaxies appear to vary along lines of constant black hole mass.

4. We have formed a composite spectrum from the spectra of five quasars whose continuum flux is detected at $\lambda \leq 584$ Å in the rest frame. We have used this composite spectrum to place a tighter limit on the optical depth of the Gunn-Peterson trough due to smoothly distributed intergalactic He I. We find that $\tau_{GP,He\,I} \leq 0.09$ at the 3 σ level.

5. We have set lower limits on the neutral hydrogen column densities of five Lyman limit systems ($0.5 \leq z_{LL} \leq 1.6$) detected in *IUE* spectra, and we briefly discuss these systems.

We thank the *IUE Observatory* staff for their help in acquiring and processing the data. We acknowledge the anonymous referee for a careful and constructive review of this work. T. M. T. also thanks Jason Cardelli and John Mathis for useful comments on the manuscript. R. F. G. and J. B. received continuing support for *IUE* observing and data reduction for this program during cycles 5–10, first under NASA grant NAG 5-38, then under interagency transfer to the NSF for NOAO. This research has made use of the NASA/IPAC Extragalactic Database (NED) which is operated by the Jet Propulsion Laboratory, California Institute of Technology, under contract with the National Aeronautics and Space Administration. We have also made use of MSEARCH at the Colorado *IUE* RDAF for retrieval of *IUE* archival data. T. M. T. is supported by the NASA Graduate Student Researchers Program through grant NGT51003. J. B. acknowledges additional support from NSF grants AST 90-58510 and RII-8800660 and NASA Long Term Astrophysics Research Program grant NAGW-2201.

REFERENCES

Antonucci, R., & Barvainis, R. 1988, ApJ, 332, L13
Avni, Y., & Tananbaum, H. 1986, ApJ, 305, 83
Bahcall, J. N., et al. 1993, ApJS, 87, 1
Bajtlik, S., Duncan, R. C., & Ostriker, J. P. 1988, ApJ, 327, 570
Baldwin, J. A. 1977, ApJ, 214, 679
Baldwin, J. A., Ferland, G. J., Martin, P. G., Corbin, M. R., Cota, S. A., Peterson, B. A., & Slettebak, A. 1991, ApJ, 374, 580
Baldwin, J. A., Wampler, E. J., & Gaskell, C. M. 1989, ApJ, 338, 630
Barvainis, R. 1993, ApJ, 412, 513
Beaver, E. A., et al. 1991, ApJ, 377, L1
Beaver, E., Burbidge, M., Cohen, R. D., Junkkarinen, V., Lyons, R., & Rosenblatt, E. 1992, in Science with the *Hubble Space Telescope*, ed. P. Benvenuti & E. Schreier (ESO Conf. and Workshop Proc. No. 44), 53
Bechtold, J. 1994, ApJS, 91, 1
Bechtold, J., Czerny, B., Elvis, M., Fabbiano, G., & Green, R. F. 1987a, ApJ, 314, 699
Bechtold, J., Green, R. F., Weymann, R. J., Schmidt, M., Estabrook, F. B., Sherman, R. D. Wahlquist, H. D., & Heckman, T. M. 1984, ApJ, 281, 76
Bechtold, J., Weymann, R. J., Lin, Z., & Malkan, M. A. 1987b, ApJ, 315, 180
Binette, L., Wang, J., Villar-Martin, M., Martin, P. G., & Magris C. G. 1993, ApJ, 414, 535
Bohlin, R. C., Harris, A. W., Holm, A. V., & Gry, C. 1990, ApJS, 73, 413
Caditz, D. 1993, ApJ, 404, 539
Calzetti, D., Kinney, A. L., & Storchi-Bergmann, T. 1994, ApJ, in press
Cardelli, J. A., & Clayton, G. C. 1991, AJ, 101, 1021
Cardelli, J. A., Clayton, G. C., & Mathis, J. S. 1989, ApJ, 345, 245
Cardelli, J. A., & Sembach, K. R. 1992, BAAS, 24, 761
Cen, R., Gnedin, N. Y., & Ostriker, J. P. 1993a, ApJ, 417, 387
Cen, R., & Ostriker, J. P. 1992a, ApJ, 393, 22
———. 1992b, ApJ, 399, 331
———. 1993, ApJ, 417, 404
Cen, R., Ostriker, J. P., & Peebles, P. J. E. 1993b, ApJ, 415, 423
Cen, R., Ostriker, J. P., Spergel, D. N., & Turok, N. 1991, ApJ, 383, 1
Cheng, F. H., & Fang, L. Z. 1987, MNRAS, 226, 485
Cheng, F. H., Gaskell, C. M., & Koratkar, A. P. 1991, ApJ, 370, 487
Clavel, J., et al. 1991, ApJ, 366, 64
Clavel, J., & Joly, M. 1984, ApJ, 131, 87
Collin-Souffrin, S. 1986, A&A, 166, 115
Crenshaw, D. M., Bruegman, O. W., & Norman, D. J. 1990, PASP, 102, 463
Cutri, R. M., Wisniewski, W. Z., Rieke, G. H., & Lebofsky, M. J. 1985, ApJ, 296, 423
Czerny, B., & Elvis, M. 1987, ApJ, 321, 305
Daltabuit, E., MacAlpine, G. M., & Cox, D. P. 1978, ApJ, 219, 372
Diplas, A., & Savage, B. D. 1994a, ApJS, 93, 211
———. 1994b, ApJ, 427, 274
Draine, B. T., & Lee, H. M. 1984, ApJ, 285, 89
Edelson, R. A., Krolik, J. H., & Pike, G. F. 1990, ApJ, 359, 86
Elvis, M., Green, R. F., Bechtold, J., Schmidt, M., Neugebauer, G., Soifer, B. T., Matthews, K., & Fabbiano, G. 1986, ApJ, 310, 291
Elvis, M., Lockman, F. J., & Wilkes, B. J. 1989, AJ, 97, 777
Espey, B. R. 1993, ApJ, 411, L59
Ferland, G. J., Korista, K. T., & Peterson, B. M. 1990, ApJ, 363, L21
Ferland, G. J., & Rees, M. J. 1988, ApJ, 332, 141
Field, G. B., & Rogers, R. D. 1993, ApJ, 403, 94
Finley, D. S., Basri, G., & Bowyer, S. 1990, ApJ, 359, 483
Fitzpatrick, E. L. 1989, in IAU Symp. 135, Interstellar Dust, ed. L. J. Allamandola & A. G. G. M. Tielens (Dordrecht: Kluwer), 37
Ginzberg, V. L., & Ozernoy, L. M. 1966, Sov. Astr.—AJ, 9, 726
Green, R. F., Pier, J. R., Schmidt, M., Estabrook, F. B., Lane, A. L., & Wahlquist, H. D. 1980, ApJ, 239, 483
Green, R. F., Schmidt, M., & Liebert, J. 1986, ApJS, 61, 305
Guilbert, P. W., & Rees, M. J. 1988, MNRAS, 233, 475
Gunn, J. E., & Peterson, B. A. 1965, ApJ, 142, 1633
Hackney, R. L., Hackney, K. R. H., & Kondo, Y. 1982, in Advances in Ultraviolet Astronomy: Four Years of IUE Research, ed. Y. Kondo, J. M. Mead, & R. H. Chapman (NASA CP-2238), 335
Hawkins, I., & Wright, E. L. 1991, in Extreme Ultraviolet Astronomy, ed. R. F. Malina & S. Bowyer (New York: Pergamon), 333
Hewitt, A., & Burbidge, G. 1987, ApJS, 63, 1
Ikeuchi, S., & Ostriker, J. P. 1986, ApJ, 301, 522
Imhoff, C. L. 1987, *IUE* NASA Newsletter, 33, 25
Jones, T. W., O'Dell, S. L., & Stein, W. A. 1974a, ApJ, 188, 353
———. 1974b, ApJ, 192, 261
Jones, T. W., & Stein, W. A. 1987, ApJ, 320, L1
Kinney, A. L. 1994 in the First Stromlo Symposium: The Physics of Active Galaxies, ed. G. V. Bicknell, M. A. Dopita, & P. J. Quinn (ASP Conf. Ser., 54), 61
Kinney, A. L., Bohlin, R. C., Blades, J. C., & York, D. G. 1991b, ApJS, 75, 645
Kinney, A. L., Bohlin, R. C., & Neill, J. D. 1988, NASA *IUE* Newsletter, 36, 114
———. 1990, in 2nd ESO/ST-ECF Data Analysis Workshop, ed. D. Baade & P. J. Grosbøl (ESO Conf. and Workshop Proc. No. 34), 73
———. 1991a, PASP, 103, 694
Kinney, A. L., Huggins, P. J., Bregman, J. N., & Glassgold, A. E. 1985, ApJ, 291, 128
Kolykhalov, P. I., & Sunyaev, R. A. 1984, Adv. Res., 3, 249
Koratkar, A. P., Kinney, A. L., & Bohlin, R. C. 1992, ApJ, 400, 435
Kormendy, J., & Djorgovski, S. 1989, ARA&A, 27, 235
Lanzetta, K. M. 1991, ApJ, 375, 1
Lanzetta, K. M., Turnshek, D. A., & Sandoval, J. 1993, ApJS, 84, 109
Laor, A. 1990, MNRAS, 246, 369
Laor, A., & Draine, B. T. 1993, ApJ, 402, 441
Laor, A., & Netzer, H. 1989, MNRAS, 238, 897
Lightman, A. L., & White, T. 1988, ApJ, 335, 57
Lynden-Bell, D. 1969, Nature, 223, 690
Lyons, R. W., Beaver, E. A., Burbidge, E. M., Cohen, R. D., & Junkkarinen, V. T. 1992, BAAS, 24, 1136
MacAlpine, G. M. 1981, ApJ, 251, 465
MacAlpine, G. M. 1985, in Astrophysics of Active Galaxies and Quasi-Stellar Objects, ed. J. S. Miller (Mill Valley: Univ. Science Books), 259
MacAlpine, G. M., Davidson, K., Gull, T. R., & Wu, C.-C. 1985, ApJ, 294, 147
Madau, P. 1992, ApJ, 389, L1
Malkan, M. A. 1983, ApJ, 268, 582
———. 1989, in Theory of Accretion Disks, ed. F. Meyer, et al. (Dordrecht: Kluwer), 19
Malkan, M. A. 1992, in Physics of Active Galactic Nuclei, ed. W. J. Duschl & S. J. Wagner (Berlin: Springer-Verlag), 109
Malkan, M. A., & Sargent, W. L. W. 1982, ApJ, 254, 22
Martin, P. G., & Rouleau, F. 1991, in Extreme Ultraviolet Astronomy, ed. R. F. Malina & S. Bowyer (New York: Pergamon), 341
Mathis, J. S. 1986, PASP, 98, 995
———. 1994, ApJ, 422, 176
Mathis, J. S., & Cardelli, J. A. 1992, ApJ, 398, 610
Mathis, J. S., Rumpl, W., & Nordsieck, K. H. 1977, ApJ, 217, 425
McKee, C. F., & Petrosian, V. 1974, ApJ, 189, 17
Melott, A. L., McKay, D. W., & Ralston, J. P. 1988, ApJ, 324, L43
Miralda-Escudé, J., & Ostriker, J. P. 1990, ApJ, 350, 1
———. 1992, ApJ, 392, 15
Møller, P., & Jakobsen, P. 1990, A&A, 228, 299
Mushotzky, R., & Ferland, G. J. 1984, ApJ, 278, 558
Nath, B. B., & Biermann, P. L. 1993, MNRAS, 265, 241
Netzer, H. 1985, ApJ, 289, 451

Netzer, H., & Laor, A. 1993, ApJ, 404, L51
Neugebauer, G., Green, R. F., Matthews, K., Schmidt, M., Soifer, B. T., & Bennett, J. 1987, ApJS, 63, 615
O'Brien, P. T., Gondhalekar, P. M., & Wilson, R. 1988a, MNRAS, 233, 845
———. 1988b, MNRAS, 233, 801
O'Dell, S. L., Scott, H. A., & Stein, W. A. 1987, ApJ, 313, 164
Osmer, P. S., & Smith, M. G. 1976, ApJ, 210, 267
———. 1977, ApJ, 213, 607
Osterbrock, D. E. 1989, Astrophysics of Gaseous Nebulae and Active Galactic Nuclei (Mill Valley: Univ. Science Books)
Pei, Y. C., Fall, S. M., & Bechtold, J. 1991, ApJ, 378, 6
Peterson, B. M. 1993, PASP, 105, 247
Pier, E. A., & Krolik, J. H. 1993, ApJ, 418, 673
Press, W. H., Teukolsky, S. A., Vetterling, W. T., & Flannery, B. P. 1992, Numerical Recipes (Cambridge: Cambridge Univ. Press)
Prévot, M. L., Lequeux, J., Maurice, E., Prévot, L., & Rocca-Volmerange, B. 1984, A&A, 132, 389
Puetter, R. C., Burbidge, E. M., Smith, H. E., & Stein, W. A. 1982, ApJ, 257, 487
Rees, M. J., Silk, J. I., Werner, M. W., & Wickramasinghe, W. C. 1969, Nature, 223, 788
Reichert, G. A., et al. 1994, ApJ, 425, 582
Reimers, D., Clavel, J., Groote, D., Engels, D., Hagen, H. J., Naylor, T., Wamsteker, W., & Hopp, U. 1989, A&A, 218, 71
Reimers, D., Vogel S., Hagen, H.-J., Engels, D., Groote, D., Wamsteker, W., Clavel, J., & Rosa, M. R. 1992, Nature, 360, 561
Rieke, G. H., & Lebofsky, M. J. 1979, ARA&A, 17, 477
Rudy, R. L. 1984, ApJ, 284, 33
Rudy, R. L., & Puetter, R. C. 1982, ApJ, 263, 43
Salpeter, E. E. 1964, ApJ, 140, 796
Sanders, D. B., Phinney, E. S., Neugebauer, G., Soifer, B. T., & Mathews, K. 1989, ApJ, 347, 29
Sargent, W. L. W., Boksenberg, A., & Steidel, C. C. 1988, ApJS, 68, 539
Sargent, W. L. W., Steidel, C. C., & Boksenberg, A. 1989, ApJS, 69, 703
Savage, B. D., Massa, D., Meade, M., & Wesselius, P. R. 1985, ApJS, 59, 397
Schmidt, M., & Green, R. F. 1983, ApJ, 269, 352
———. 1986, ApJ, 305, 68
Schneider, D. P., et al. 1993, ApJS, 87, 45
Sciama, D. W. 1988, MNRAS, 230, 13P
———. 1990, ApJ, 364, 549
Shapiro, P. R., & Giroux, M. L. 1987, ApJ, 321, L107
Shields, G. A. 1978, Nature, 272, 706
Shuder, J. M., & MacAlpine, G. M. 1979, ApJ, 230, 348
Snijders, M. A. J. 1983, *IUE* NASA Newsletter, 23, 56
Stark, A. A., Gammie, C. F., Wilson, R. W., Bally, J., Linke, R. A., Heiles, C., & Hurwitz, M. 1992, ApJS, 79, 77
Stecher, T. P., & Donn, B. 1965, ApJ, 142, 1681
Sun, W. H., & Malkan, M. A. 1987, in Astrophysical Jets and Their Engines, ed. W. Kundt (Dordrecht: Reidel), 125
———. 1989, ApJ, 346, 68
Tananbaum, H., Avni, Y., Green, R. F., Schmidt, M., & Zamorani, G. 1986, ApJ, 305, 57
Terasawa, N. 1992, ApJ, 392, L15
Tripp, T. M., Green, R. F., & Bechtold, J. 1990, ApJ, 364, L29
Urry, M., & Reichert, G. 1988, NASA *IUE* Newsletter, 34, 95
Wandel, A. 1991, A&A, 241, 5
Wandel, A., & Petrosian, V. 1988, ApJ, 329, L11
Wu, C.-C., Boggess, A., & Gull, T. R. 1983, ApJ, 266, 28
Young, P., Sargent, W. L. W., & Boksenberg, A. 1982, ApJS, 48, 455
Zheng, W., & Malkan, M. A. 1993, ApJ, 415, 517